Integrated provenance analysis of a convergent retroarc foreland system: U–Pb ages, heavy minerals, Nd isotopes, and sandstone compositions of the Middle Magdalena Valley basin, northern Andes, Colombia

Junsheng Nie [a,b,*], Brian K. Horton [a,c], Joel E. Saylor [a], Andrés Mora [d], Maria Mange [e], Carmala N. Garzione [f], Asish Basu [f], Christopher J. Moreno [a], Victor Caballero [d], Mauricio Parra [a,d]

[a] Department of Geological Sciences, Jackson School of Geosciences, University of Texas at Austin, Austin, TX 78712, USA
[b] MOE Key Laboratory of Western China's Environmental System, Research School of Arid Environment and Climate Change, Lanzhou University, Lanzhou, Gansu 730000, China
[c] Institute for Geophysics, Jackson School of Geosciences, University of Texas at Austin, Austin, TX 78712, USA
[d] Instituto Colombiano del Petróleo, Ecopetrol, Bucaramanga, Colombia
[e] Department of Geology, University of California, Davis, CA 95616, USA
[f] Department of Earth and Environmental Sciences, University of Rochester, Rochester, NY 14627, USA

ARTICLE INFO

ABSTRACT

Sediment provenance analysis remains a powerful method for testing hypotheses on the temporal and spatial evolution of uplifted source regions, but issues such as recycling, nonunique sources, and pre- and post-depositional modifications may complicate interpretation of results from individual provenance techniques. Convergent retroarc systems commonly contain sediment sources that are sufficiently diverse (continental magmatic arc, fold–thrust belt, and stable craton) to enable explicit provenance assessments. In this paper, we combine detrital zircon U–Pb geochronology, heavy mineral identification, Nd isotopic analyses, conventional sandstone petrography, and paleocurrent measurements to reconstruct the clastic provenance history of a long-lived sedimentary basin now exposed in an intermontane zone of the northern Andean hinterland of Colombia. The Middle Magdalena Valley basin, situated between the Central Cordillera and Eastern Cordillera, contains a 5–10 km-thick succession of Upper Cretaceous to Quaternary fill. The integrated techniques show a pronounced change in provenance during the Paleocene transition from the lower to upper Lisama Formation. We interpret this as a shift from an eastern cratonic source to a western Andean source composed of magmatic-arc rocks uplifted during initial shortening of the Central Cordillera. The appearance of detrital chloritoid and a shift to more negative $\varepsilon_{Nd(t=0)}$ values in middle Eocene strata of the middle La Paz Formation are attributed to shortening-related exhumation of a continental basement block (La Cira–Infantas paleo-high), now buried, along the axis of the Magdalena Valley. The diverse provenance proxies also show distinct changes during middle to late Eocene deposition of the Esmeraldas Formation that likely reflect initial rock uplift and exhumation of the fold–thrust belt defining the Eastern Cordillera. Upsection, detrital zircon U–Pb ages and heavy mineral assemblages for Oligocene and younger clastic deposits indicate that the Mesozoic sedimentary cover of the Eastern Cordillera was recycled during continued Cenozoic shortening. Our multidisciplinary provenance study refines the tectonic history of the Colombian Andes and demonstrates that uncertainties related to sediment recycling, nonunique sources, source heterogeneity, and climate in interpreting provenance data can be minimized via an integrated approach.

© 2011 Elsevier B.V. All rights reserved.

Contents

* Corresponding author at: Research School of Arid Environment and Climate Change, Lanzhou University, Lanzhou, Gansu 730000, China. Tel.: +86 18794804964.
E-mail address: niejunsheng@gmail.com (J. Nie).

1. Introduction

Sediment provenance analyses are routinely applied to solve diverse geological problems. Notable themes include the unroofing histories of individual thrust sheets (DeCelles, 1988; Najman et al., 2009; Lawton et al., 2010) or extensional fault blocks (Horton and Schmitt, 1998), estimates of fault displacement (Niemi et al., 2001; Gehrels et al., 2003; Yue et al., 2005), orogen-scale exhumation records (DeCelles et al., 1998; Najman and Garzanti, 2000), terrane/plate reconstructions (McClelland et al., 1992; Ross et al., 1992; Carroll et al., 1995; DeCelles et al., 2000; Thomas et al., 2004; Weislogel et al., 2006), and continent-scale dispersal patterns (Rainbird et al., 1992; Riggs et al., 1996; Dickinson and Gehrels, 2003). In the past decade, provenance analysis incorporating detrital ziron U–Pb geochronology has become an increasingly important technique (Davis and Lin, 2003; Davis et al., 2003; Fedo et al., 2003; Chang et al., 2006; Gehrels et al., 2006).

However, provenance studies are subject to limitations, a partial list of which includes: (1) nonunique sediment sources (i.e., comparable signatures from different localities) (DeCelles, 1988; Steidtmann and Schmitt, 1988; Cowan et al., 1997; Pe-Piper et al., 2008); (2) internal variability within a single source area, including uneven zircon fertility and Nd isotopic heterogeneity (Condie, 1998; Eriksson et al., 2003; Link et al., 2005; Moecher and Samson, 2006; Dickinson, 2008); (3) incomplete characterization of potential sources (Amidon et al., 2005a); (4) sediment routing complexity (Allen, 2008); (5) sediment recycling (Johnsson, 1993; Cox et al., 1995; Dickinson et al., 2009); (6) climatic and erosion/weathering effects (Suttner et al., 1981; Suttner and Basu, 1985; Johnsson, 1993; Amidon et al., 2005a, 2005b); (7) grain attrition during transport (Cox and Lowe, 1995; Nesbitt and Young, 1996); (8) hydraulic sorting according to depositional processes (Garzanti et al., 2008; Ohta, 2008; Garzanti et al., 2009; Lawrence et al., 2011); and (9) post-depositional (diagenetic) alteration (Milliken, 1988; Fedo et al., 1995).

Given these extensive caveats, successful provenance applications involve cases where differentiable source regions enable formulation of distinct and testable hypotheses. Uncertainties in provenance interpretations may be reduced further through the combination of different viable techniques, including: (1) sandstone compositional studies (Dickinson and Suczek, 1979; Dickinson et al., 1983; Ingersoll et al., 1984); (2) heavy mineral identification (Amano and Taira, 1992; Morton and Hallsworth, 1994; Uddin and Lundberg, 1998; Morton and Hallsworth, 1999; Koschinsky et al., 2001; Mange and Otvos, 2005; Mange et al., 2005; Kempf et al., 2009; Pindell et al., 2009; Garzanti et al., 2010; Vezzoli et al., 2010; Zahid and Barbeau, 2010); (3) isotope geochemistry (Basu et al., 1990; Linn et al., 1992; Derry and France-Lanord, 1996; Johnson and Winter, 1999; Robinson et al., 2001; Garzione et al., 2005); (4) major and trace-element geochemistry (Roser and Korsch, 1988; McLennan, 1989; Hoskin and Ireland, 2000; von Eynatten, 2003); and (5) geochronology and thermochronology (Copeland and Harrison, 1990; Gallagher et al., 1998; Bernet et al., 2001; Reiners et al., 2005; Chew et al., 2008; Dickinson and Gehrels, 2008; Carrapa et al., 2009; Horton et al., 2010a). In some cases, analyses of modern river systems (Cullers et al., 1988; Link et al., 2005) can be united with ancient basin

Fig. 1. (A) Map showing tectonomorphic provinces of the northern Andes. White dots (R1–R6) show locations of modern river samples taken for detrital zircon U–Pb dating (R1, R2, R3, R5, and R6) and heavy mineral analyses (R1, R3, R4, R5, and R6). WC: Western Cordillera. CC: Central Cordillera. EC: Eastern Cordillera. CV: Cauca Valley. (B) Simplified geologic map of the Middle Magdalena Valley basin (MMVB), showing study region along the eastern limb of Nuevo Mundo syncline. NW–SE line shows approximate location of stratigraphic section yielding sandstone and mudstone samples for detrital zircon U–Pb geochronology, Nd isotope, petrography, and heavy mineral analysis. Panel A is revised from Moreno et al. (2011).
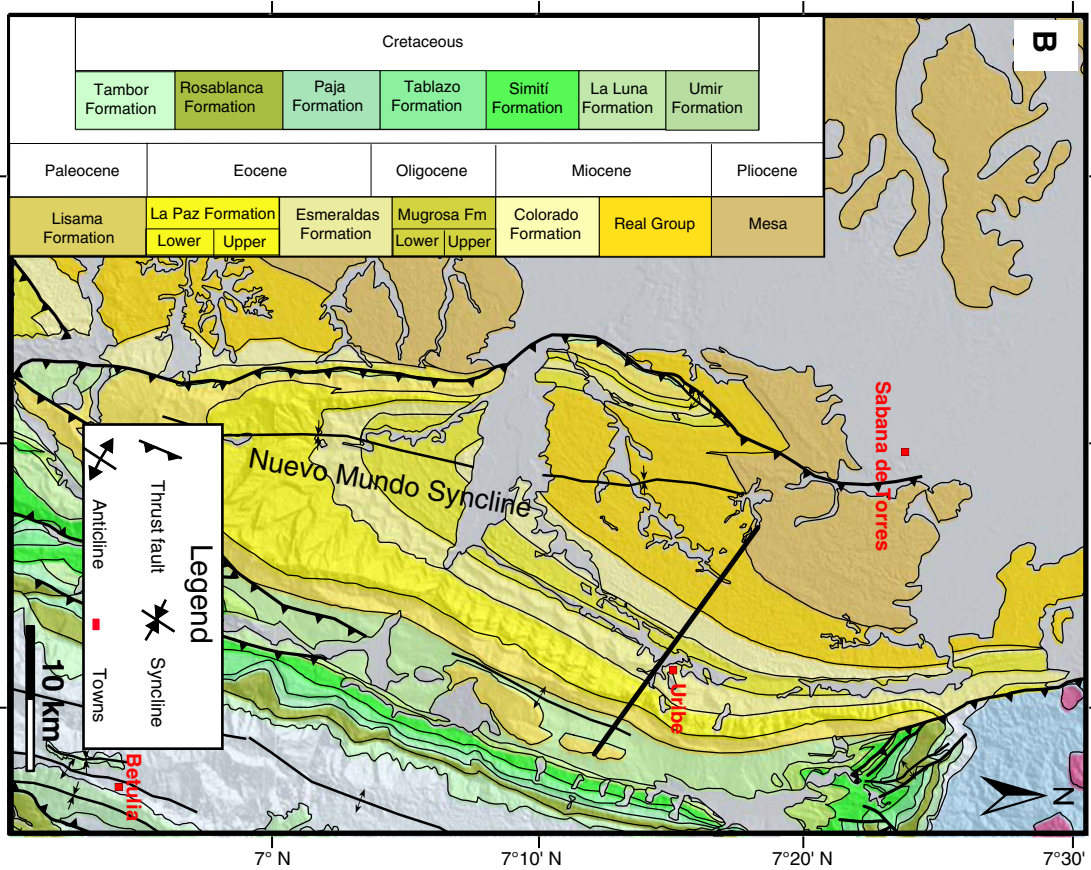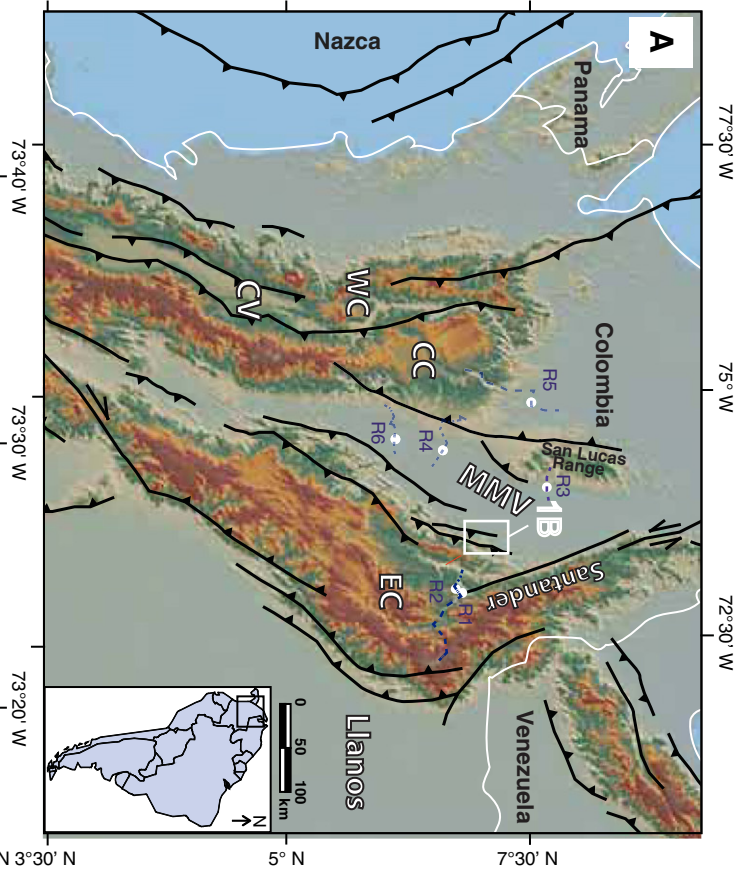
Provenance		Detrital zircon U/Pb age spectra	ε_{Nd}	Heavy mineral assemblage	Heavy mineral morphology	Sandstone composition
A	Craton	Precambrian-age dominated	≤ -12.7	higher proportion of stable minerals (zircon, tourmaline, and rutile)	higher proportion of rounded grains	quartz and metamorphic lithic rich
B	Magmatic arc	Phanerozoic-age dominated	≥ -12.7	lower proportion of stable minerals (zircon, tourmaline, and rutile)	higher proportion of euhedral grains	volcanic lithic and feldspar rich
C	Fold-thrust belt	mixed	intermediate	intermediate	mixed	sedimentary lithic and quartz rich

Fig. 2. Predicted sediment provenance signatures for different components of a continental convergent retroarc setting: (A) stable craton source; (B) magmatic arc source; (C) fold–thrust belt source. The $\varepsilon_{Nd(t=0)}$ cutoff value of -12.7 is specific to the Amazonian craton of South America (Basu et al., 1990).

fill to characterize sediment sources and track long-term evolution of source regions.

In this paper, we assess the Cenozoic provenance history of an Andean retroarc sedimentary basin in tropical Colombia through a combination of detrital zircon U–Pb geochronology, heavy mineral identification, Nd isotopic analyses, paleocurrent measurements, and sandstone petrography of sedimentary rocks and selected modern river sediments. Previous provenance studies in the region are limited, partially because of the strong climatic overprint that may mask the original source signals (e.g., Johnsson et al., 1988). Our study of the Middle Magdalena Valley basin (MMVB) in the northern Andes of Colombia (Fig. 1) is developed on a framework of discrete testable hypotheses that capitalize on the considerable regional variations in potential source regions in northwestern South America—namely a stable craton, continental magmatic arc, and retroarc fold–thrust belt (Fig. 2). Uncertainties related to sediment recycling, non-unique source regions, source heterogeneity, and climate conditions can be addressed through parallel application of multiple provenance techniques. This integrated provenance strategy proves valuable in evaluating the exhumation history of mountain ranges bounding the MMVB, and should shed light on the geologic histories of similar tectonic settings.

2. Regional geologic setting and potential sediment sources

The northernmost segment of the ~7000-km-long Andean mountain chain consists of three discrete ranges bounded by intermontane valleys and basins (Fig. 1A). Each of these ranges—the Western Cordillera, Central Cordillera, and Eastern Cordillera (hereafter WC, CC, and EC, respectively)—has its own geologic history and combination of crystalline basement and younger igneous and sedimentary rocks. The WC, CC, and EC ranges are further distinguished from the stable craton, the Guyana shield, exposed to the east in the Amazon and Orinoco drainage basins (Fig. 1A).

The WC is composed of Late Cretaceous–Cenozoic igneous rocks principally of oceanic affinity (Aspden et al., 1987). In contrast, the CC has pre-Mesozoic, low- to high-grade metamorphic basement of mixed continental and oceanic origin that is intruded by numerous Mesozoic–Cenozoic plutons of the Andean magmatic arc (Aspden and McCourt, 1986; Aspden et al., 1987; Gómez et al., 2005). Finally, the EC has crystalline continental basement of Proterozoic to early Paleozoic age. The EC basement is covered mostly by Paleozoic–Mesozoic strata, with exposure of basement mainly in the Santander, Garzon, and Santa Marta massifs (Dengo and Covey, 1993; Gómez et al., 2005). The Llanos foreland basin defines the lowland region east of

the northern Andes of Colombia. Along the distal eastern margin of the Llanos basin, exposures of principally Precambrian basement define the Guyana shield, which represents the northern part of the Amazonian craton.

The focus of this study is the MMVB (Fig. 1), a retroarc sedimentary basin between the CC and EC. Previous studies have established the MMVB as a multi-phase successor basin whose history includes Jurassic–Early Cretaceous rifting, Late Cretaceous thermal subsidence, and latest Cretaceous–Eocene incorporation into a regionally extensive foreland basin that was partitioned during Cenozoic Andean shortening, crustal thickening, and flexural subsidence (Cooper et al., 1995; Villamil, 1999; Gómez et al., 2003, 2005; Sarmiento-Rojas et al., 2006; Bayona et al., 2008; Horton et al., 2010a; Saylor et al., 2011). The persistence of Mesozoic–Cenozoic sediment accumulation in the MMVB makes the location a unique sedimentary record of long-term construction of the northern Andes.

In addition to the diverse sediment sources (WC, CC, EC, and craton), the Colombian Andes are distinguished by extremely high precipitation (among the highest on Earth) and a significant rainfall gradient (Mora et al., 2008; Saylor et al., 2009). As a result of easterly winds, the deeply incised eastern part of the EC receives ~5–7 m of annual precipitation whereas low-relief regions of the western part of the EC and MMVB only receive ~1–2 m. This extreme climate gradient coupled with intense tropical weathering may lead to the perception that the region is poorly suited for sedimentary provenance studies. Therefore, in addition to concerns over sediment recycling and complex source regions, a successful provenance approach should be able to account for a potential climate signal or demonstrate that available provenance proxies are unaffected by climate change.

3. Middle Magdalena Valley basin stratigraphy

The Nuevo Mundo syncline, a type locality of MMVB strata, contains a nearly continuous clastic succession of uppermost Cretaceous through Cenozoic basin fill (Fig. 3). The Maastrichtian Umir Formation and overlying Paleocene Lisama Formation record the transition from shallow marine to deltaic and alluvial plain environments (Gómez et al., 2005; Moreno et al., 2011). The lower–middle Eocene La Paz Formation conformably overlies the Lisama Formation on the eastern limb of the syncline. Amalgamated lenticular sandstone bodies and subordinate mudstones of the La Paz Formation are of fluvial origin (Gómez et al., 2005). In the upper Eocene–lower Oligocene Esmeraldas Formation, broadly lenticular fluvial sandstones are separated by greater proportions of fine-grained overbank deposits than

Fig. 3. Stratigraphic log for the ~7-km-thick succession along the eastern limb of the Nuevo Mundo syncline showing relative levels of Cretaceous–Miocene samples for detrital zircon U–Pb geochronology (Z1–Z13), Nd isotopes (N1–N8), heavy mineral analyses (H1–H11), and sandstone petrography analyses. Grain sizes: cl: clay; si: silt; ss: sandstone: cg: conglomerate. Highly schematic stratigraphic log for the Umir Formation is simplified from Morales (1958) and Rangel et al. (2002). Rose diagrams summarize paleocurrent data from Moreno et al. (2011) and Caballero et al. (2010).
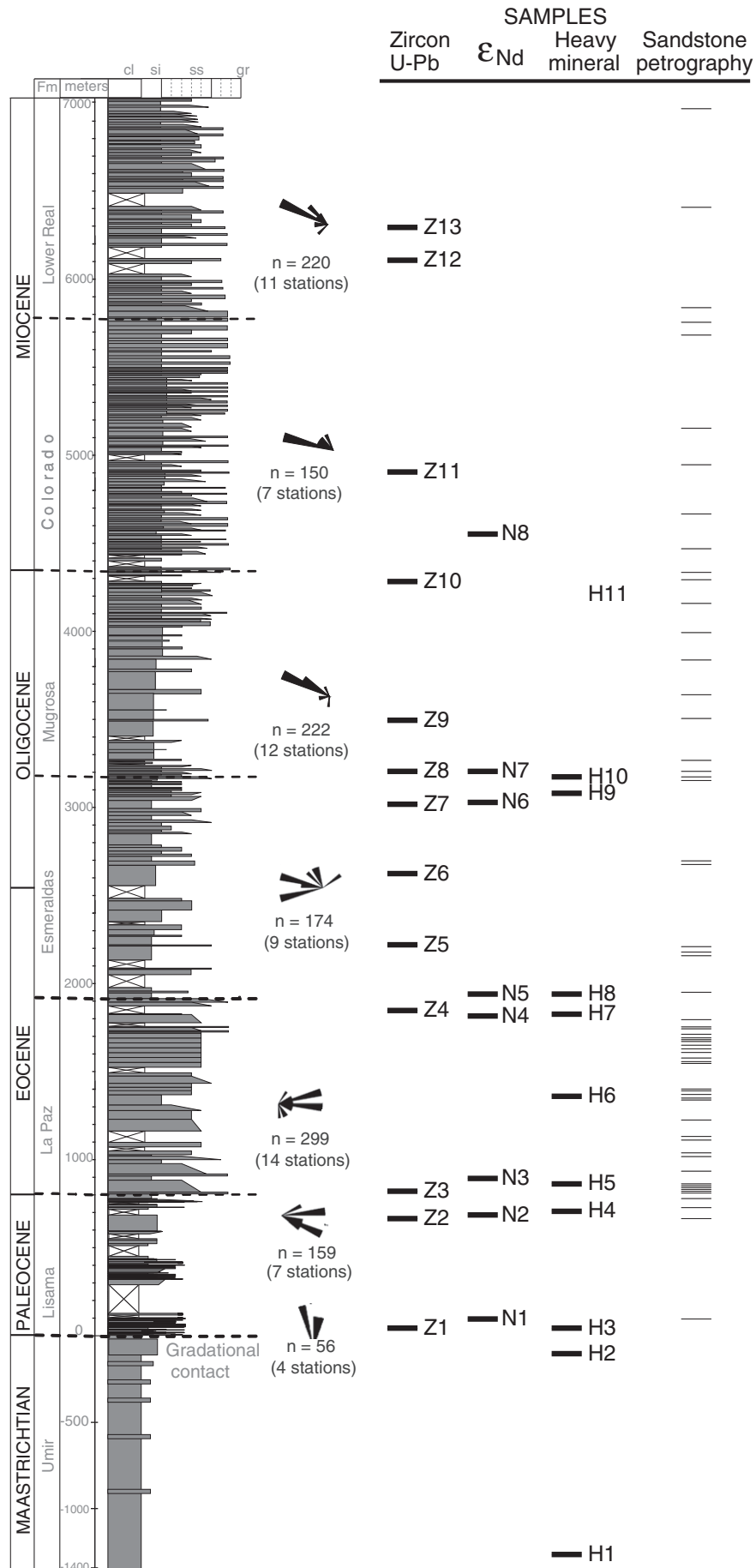
the underlying La Paz Formation. The upper Oligocene Mugrosa Formation is characterized by well-developed pedogenic features which overprint the upward-coarsening succession of channel sandstones and floodplain mudstones. The contact between the Mugrosa Formation and the lower–middle Miocene Colorado Formation is transitional. The upward coarsening trend and extensive pedogenic features continue upsection into the Colorado Formation, which culminates in alluvial-fan conglomerates. The upper Miocene Real Formation is distinguished from the Colorado Formation by a greater proportion of volcanic detritus.

Paleocurrent data from the studied section (Caballero et al., 2010; Moreno et al., 2011) indicate axial northward transport for the lower Lisama Formation, transverse eastward transport for the upper Lisama Formation, dominantly eastward flow for the La Paz and lower Esmeraldas formations, variable but principally westward flow for the middle to upper Esmeraldas Formation, and generally northwestward transport, for the Mugrosa, Colorado, and Real formations. These data supplement existing regional syntheses of sediment dispersal patterns across the Colombian Andes and Llanos basin (e.g., Cooper et al., 1995; Villamil, 1999; Gómez et al., 2003, 2005; Bayona et al., 2008).

4. Provenance hypotheses

Contrasting crustal histories for cratons, magmatic arcs, and fold–thrust belts generate distinct ages, lithologies, and chemical compositions. This enables explicit hypotheses for convergent retroarc systems that are testable through a combination of established provenance techniques (Fig. 2). Here, we outline several hypotheses specific to the northern Andes and the adjacent craton (Guyana shield) of northern South America. Comparable provenance hypotheses could be posed for most basins in ocean-continent convergent systems. In this study, each hypothesis makes predictions for the expected detrital zircon U–Pb age signatures, heavy mineral assemblages, Nd isotopic ratios, sandstone compositions, and paleocurrents.

4.1. Stable craton

In northern South America, an exclusively cratonic source in more eastern regions (Fig. 2A) would be characterized by Precambrian zircon U–Pb ages ($>$600 Ma, mainly Grenville age and other Precambrian ages of $>$2300, 1600–1450, 1350–1250 Ma) (Priem et al., 1989; Teixeira et al., 1989; Goldstein et al., 1997; Restrepo-Pace et al., 1997; Cordani et al., 2000; Chew et al., 2007; Horton et al., 2010b), lower Nd isotopic ratios and thus more negative $\varepsilon_{Nd(t=0)}$ values (≤ -12.7) (Basu et al., 1990), moderate- to high-grade metamorphic lithologies with granitic contributions, lower proportions of euhedral and angular grains relative to rounded grains (due to long-distance transport and multiple-phase recycling), and sandstones rich in quartz and metamorphic lithic fragments.

4.2. Magmatic arc

A magmatic arc source from the western flank of the northern Andes (Fig. 2B) would be dominated by Phanerozoic zircon U–Pb ages (primarily Mesozoic–Cenozoic igneous rocks related to subduction of a Pacific-affinity oceanic plate (e.g., modern Nazca plate)) (McCourt et al., 1984; Aspden et al., 1987), more juvenile crustal signatures ($\varepsilon_{Nd(t=0)} \geq -12.7$) (Basu et al., 1990), igneous- and metamorphic-derived heavy mineral assemblages, lower proportions of stable heavy minerals (zircon, tourmaline, and rutile), higher proportions of euhedral and angular grains, and sandstones rich in feldspar and volcanic lithic fragments. Although possible, most workers consider it unlikely that sediment derived from the WC reached the MMVB. Nevertheless, if so, these sediments would be distinctive because the WC is an accreted oceanic terrane of latest Cretaceous–

Eocene age with post-collisional magmatism concentrated at 25–10 Ma (Aspden et al., 1987).

4.3. Fold–thrust belt

A retroarc fold–thrust belt source in the northern Andes would consist of signals from a mixture of the two previous endmembers. Because of its geologic history, the EC fold–thrust belt in Colombia represents an intermediate hypothesis (Fig. 2C) between the cratonic endmember (Fig. 2A) and magmatic-arc endmember (Fig. 2B). Specifically, the EC is dominated by sedimentary rocks that have, at varying times, been derived from either an eastern cratonic source (accumulation of 3–8 km of Cretaceous sediment) or western arc assemblage (accumulation of 2–3 km of Paleogene sediment) (Horton et al., 2010b; Saylor et al., 2011). In this sense, the EC should represent a mixed assemblage with cratonic and arc signatures. Although restricted in area, most basement massifs in the EC reveal lower Paleozoic ages with Grenville inheritance, except for the Late Triassic-Early Jurassic ages of the Santander massif in the northernmost EC (Restrepo-Pace et al., 1997; Horton et al., 2010b). A fold–thrust belt source would be dominated by zircon U–Pb ages of cratonic, CC, and local EC basement (200 Ma, 400–500 Ma, and 900–1200 Ma), $\varepsilon_{Nd(t=0)}$ values near -12.7 (Basu et al., 1990), mixed heavy mineral compositions of cratonic, magmatic arc (CC) sources, and local basement (EC) sources, and sandstone components rich in quartz and lithic sedimentary fragments.

4.4. Hypothesis refinement

We present the hypotheses above as a foundation requiring refinement in order to construct an accurate provenance history of the MMVB. This approach allows us to incorporate geologic constraints from previous studies to best delineate the complex spatial and temporal variations of deformation and denudation. Building on previous studies, we summarize the following geologic history. A period of Jurassic–Early Cretaceous continental extension affected the region occupied by the present Colombian Andes (Cooper et al., 1995; Sarmiento-Rojas et al., 2006). Post-rift thermal subsidence during Late Cretaceous and possibly early Paleogene time generated a very broad region of low topography (including the entire EC) containing sediment originating from both the eastern craton and western magmatic arc(s) (Cooper et al., 1995; Gómez et al., 2003; Horton et al., 2010b). At some point in Late Cretaceous to Oligocene time, shortening began in the arc and on its eastern flank, creating a major sediment source in the west that is approximated by the present CC (Cooper et al., 1995; Gómez et al., 2003, 2005; Horton et al., 2010b). A major unconformity in the subsurface of the MMVB bevels crystalline basement and is overlapped by upper Eocene–Oligocene strata (Gómez et al., 2003, 2005). These relationships require an initial phase of rock uplift and exhumation (*sensu* England and Molnar, 1990) of the MMVB basement. Finally, initial shortening-related exhumation began in the EC fold–thrust belt at some point in the mid to late Cenozoic (Dengo and Covey, 1993; Gregory-Wodzicki, 2000; Mora et al., 2006; Mora et al., 2008; Parra et al., 2009). Surface uplift of the EC generated a sufficiently large topographic feature that partitioned the preexisting foreland basin into a western hinterland basin (Magdalena Valley basin) and an eastern foreland basin (Llanos basin), both of which were fed largely by clastic sediment derived from erosion of the EC (Fig. 1A).

5. Sampling

U–Pb geochronology based on laser-ablation–inductively coupled plasma–mass spectrometry (LA–ICP–MS) is well suited for analysis of zircons $>$50 μm in diameter, although recent progress has made it possible to measure smaller grains (Johnston et al., 2009). Density of zircon (4850 kg/m^3) far exceeds that of quartz (2650 kg/m^3), so

hydraulically equivalent zircon grains are expected to be approximately one phi size smaller than accompanying quartz grains (Komar, 2007). Therefore, we collected ~5 kg of medium- to coarse-grained sandstone per sample in order to obtain sufficiently sized zircons (>50 μm) for U–Pb analyses. For heavy mineral analysis, we collected fine- to medium-grained sandstone because the coarser fractions may be preferentially enriched in one or two species but lacking in others (Komar, 2007). For Nd isotopic analyses, we sampled mudstone following protocols established in previous studies (Linn et al., 1992; Derry and France-Lanord, 1996; Johnson and Winter, 1999; Robinson et al., 2001; Garzione et al., 2005).

Samples were collected from the eastern limb of the Nuevo Mundo syncline in the northern MMVB, a type locality for Cenozoic fill of the MMVB intermontane basin (Morales, 1958; Gómez et al., 2005) (Figs. 1B and 3). We obtained 13 sandstone samples for detrital zircon U–Pb analyses, 8 mudstone samples for Nd analyses, and 11 fine- to medium-grained sandstone samples for heavy mineral analyses (Fig. 3). We also collected samples of unconsolidated sand from five modern rivers (Fig. 1A) for zircon U–Pb and heavy mineral analyses: the Rio Manco and Rio Umbala draining the northernmost EC (Santander massif) and the Rio Santo Domingo, Rio Nechi, Rio Nare, and Rio Swan draining the CC. We also collected 65 samples of medium-grained sandstones for sandstone petrography. A synthesis of recent paleocurrent and sandstone petrographic data from Caballero et al. (2010) and Moreno et al. (2011) are included here to enable comparison with the additional provenance proxies.

6. Rationale and methods

In situations where different source regions have experienced contrasting geological histories, there is a potential to test competing hypotheses by exploiting the differences in zircon U–Pb ages, Nd isotope values, sandstone compositions, and heavy mineral assemblages. When these source regions are exhumed, their geological fingerprints are assumed to be maintained during transport and deposition. However, alteration or selective processes during weathering, erosion, transport, deposition, and post-depositional burial may disrupt the anticipated detrital signatures of different sediment source regions. Nevertheless, we emphasize that the three principal source regions in retroarc convergent systems—namely the stable craton, magmatic arc, and fold–thrust belt—are sufficiently distinct that these sources commonly can be discriminated despite modest departures from the original source compositions.

6.1. Detrital zircon U–Pb geochronology

6.1.1. Rationale
Crustal rocks generally contain zircons resistant to chemical weathering and post-depositional diagenetic processes. In cases where possible sources exhibit diagnostic zircon U–Pb age distribution patterns, one can infer the original source by dating zircons from basin fill. In retroarc settings, where sediments originate from a stable craton, magmatic arc, or fold–thrust belt with their unique zircon age distribution patterns, detrital zircon U–Pb ages provide an excellent means to discriminate sediment provenance from these sources. Limitations to this method arise where different source regions have similar zircon U–Pb age signatures. Other factors such as zircon fertility of source rocks, sedimentary routing changes, and recycling will also complicate the interpretation of zircon age distributions. Ultimately, comparing provenance histories based on zircon U–Pb ages with other provenance proxies can narrow down this complexity and improve interpretations.

Detrital zircon U–Pb data are often presented as age probability plots and age bin histograms. Whereas histograms do not consider age uncertainties, age probability plots incorporate such uncertainties

(Vermeesch, 2004) and, therefore, represent a more robust presentation of the data (Dickinson and Gehrels, 2008).

6.1.2. Methods
Detrital zircon grains were separated by standard heavy liquid techniques, selected randomly, and imaged using cathodoluminescence. Samples Z1–Z5 and Z10–Z13, and river samples R2 (Rio Umbala), R3 (Rio Santo Domingo) and R5 (Rio Nechi) were analyzed by LA–ICP–MS using a GVI Isoprobe in the Department of Geological Sciences at the University of Texas at Austin (UT). Samples Z6–Z9 and river sample R1 (Rio Manco, EC) and R6 (Rio Nare, CC) were analyzed by LA–ICP–MS in the Arizona LaserChron Center (ALC) at the University of Arizona. Following standard data filters of the UT lab, we report analyses between 40% and −20% discordant for ages older than 500 Ma, between 65% and −20% discordant for ages younger than 500 Ma, and remove analyses exceeding a 25% uncertainty filter (1σ) from further consideration. For samples analyzed at the ALC, we followed standard data filters of the lab, reporting age analyses that yield between 10% and −5% discordance for ages older than 1000 Ma, with a 10% uncertainty filter (1σ). For all analyses, discordance was calculated on the basis of $^{206}Pb/^{238}U$ and $^{207}Pb/^{206}Pb$ ages.

Results for each sample are plotted as relative age probability diagrams (Ludwig, 2003) and age histograms (Figs. 4 and 5). Following protocols established in previous studies, age peaks on age probability diagrams are considered significant only if defined by 3 or more analyses (Gehrels et al., 2006; Dickinson and Gehrels, 2008). Although inclusion of some discordant analyses adds some degree of scatter to the age spectra, this has little impact on the interpretation of detrital zircon populations, which represent comparisons based on clusters of grain ages rather than on individual ages.

6.2. Heavy mineral analysis

6.2.1. Rationale
High-resolution heavy mineral analysis is based on the concept that detrital heavy mineral assemblages are generally complex and that individual species in most cases are represented by diagnostic optical, chemical, morphological, and structural varieties. The chemistry and crystal forms of these varieties are controlled by the specific pressure, temperature, and fluid conditions during crystallization in their parent rocks, with further diversification caused by subsequent sedimentary processes (Mange-Rajetzky, 1995; Mange and Wright, 2007). Distinguishing species that are highly resistant chemically, such as zircon, tourmaline, rutile, and possibly apatite, offers the greatest advantage because these varieties are ubiquitous and largely unaffected by burial diagenesis. Moreover, consideration of several different categories of individual species reduces the potential influence of hydraulic and diagenetic factors (Morton, 1985).

Heavy mineral varieties can be either (a) provenance-diagnostic, facies-independent, or (b) facies-sensitive. Provenance-diagnostic signatures such as color, inclusions, and internal structure remain unchanged during sedimentation and after burial, rendering them critical for source area reconstruction. Facies-sensitive properties such as morphology, grain size, and surface textures may be adversely affected by transport, recycling, and diagenesis and dissolution.

6.2.2. Methods
Sample preparation and heavy liquid separations were conducted using methods described by Mange and Maurer (1992): (a) disaggregation of sandstones; (b) wet sieving (0.063 mm aperture) to remove clay and silt particles; (c) standard dry sieving retaining the 0.063–0.212 mm size fractions; (d) separation of heavy minerals in a low-viscosity sodium polytungstate (density 2820 kg/m^3) using a centrifuge and partial freezing method; and (e) acid digestion using 10% acetic acid to dissolve carbonates.
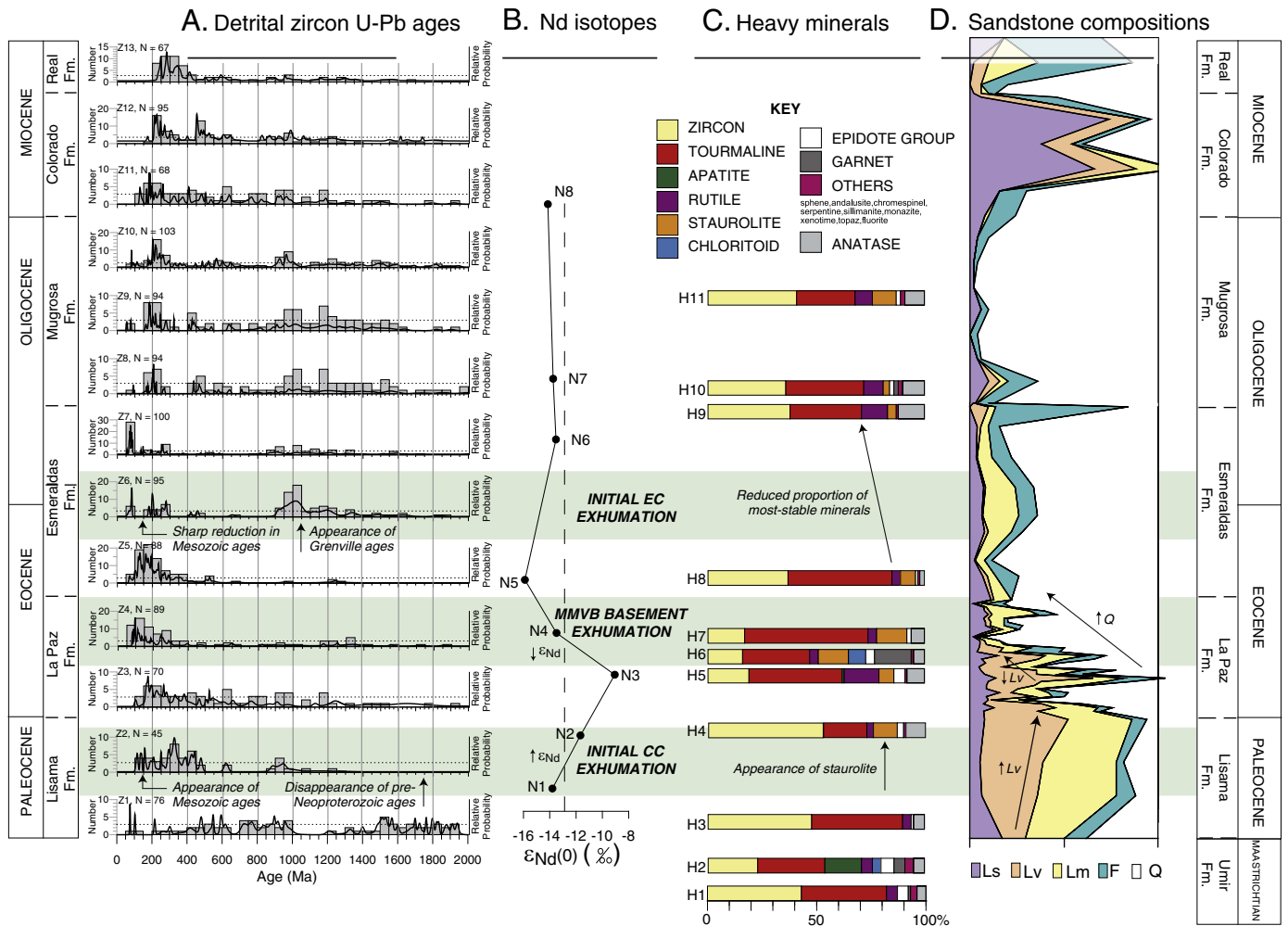
Fig. 4. Composite plot of provenance data for samples shown in Fig. 3, including (A) detrital zircon U–Pb age spectra depicted as age probability functions (thick lines) and age histograms (gray bars), (B) $\varepsilon_{Nd(t=0)}$ results with a −12.7 reference value (dashed vertical line) plotted for a representative granite from the Brazilian craton (Basu et al., 1990), (C) heavy mineral assemblages, and (D) sandstone petrography compositions. Note that scale of age probability function curves has been adjusted to fit the figure and thus area under the age probability function curves is not equal for each sample. In (D), principal categories include quartz (Q), feldspar (F), and lithic fragments of volcanic (Lv), metamorphic (Lm), and sedimentary (Ls), where Q = Qm + Qp + Qpt + Lch. Arrows and green shadow bars highlight significant changes mentioned in text.

Each heavy mineral concentrate was mounted in liquid Canada balsam on a glass slide for identification mineralogy and grain morphology under the polarizing light microscope. Grain counting was made along parallel bands on the slide ("ribbon counting" method of Galehouse, 1971). Components of the non-opaque heavy mineral suite were not counted, thus excluding micas. However, the presence and abundance of various micas, opaque grains, and authigenic phases were recorded.

During the first stage of microscopy, the frequencies of individual heavy minerals were point counted using a conventional, species-level identification. After 200 grains were counted, the ensuing point-counting technique focused on varietal differentiation. Depending on grain availability, 50–75 grains each of zircon and tourmaline were recorded, allocating them into discrete varietal categories. Raw data from the point counting program were then recalculated as percentage values and tabulated.

6.3. Nd isotope and trace element analysis

6.3.1. Rationale

Sm and Nd are chemically similar rare earth elements (REE) that experience negligible fractionation during processes such as weathering, sediment transport, and deposition of fine-grained clastic material (Taylor and McLennan, 1985). Therefore, Nd isotopic compositions

of basin-fill mudstones can be compared to the signatures of their possible source regions to identify the original source of fine-grained clastic material.

Sm has seven naturally occurring isotopes. Of these, ^{147}Sm, ^{148}Sm, and ^{149}Sm are all radioactive, but only the half life of ^{147}Sm (10^6 Gyr) is sufficiently short to produce small but measurable ^{143}Nd over periods of several million years. This provides the basis for the Sm–Nd dating method. Both Nd and Sm are incompatible elements but Nd is more incompatible than Sm, and will be more enriched in a partial melt than Sm. Therefore, crust formed by partial melting of the mantle will have a low Sm/Nd ratio and a negative εNd value (DePaolo, 1981). Partial melting has depleted the mantle relatively more in Nd than in Sm, so the depleted mantle has a higher Sm/Nd ratio than crust and a positive εNd value. Similar patterns hold for magmatic rock derived recently from the mantle.

6.3.2. Methods

Trace elements were analyzed with an inductively coupled plasma mass spectrometer (ICP-MS PQ II+) at the University of Massachusetts Amherst, and Nd isotopic ratios were determined with a VG Sector thermal ionization mass spectrometer at the University of Rochester. For ICP-MS analyses, 100 mg of powder was dissolved in Teflon bombs, diluted to 100 mL in a 5% HNO₃ solution with a 10 ppb internal standard
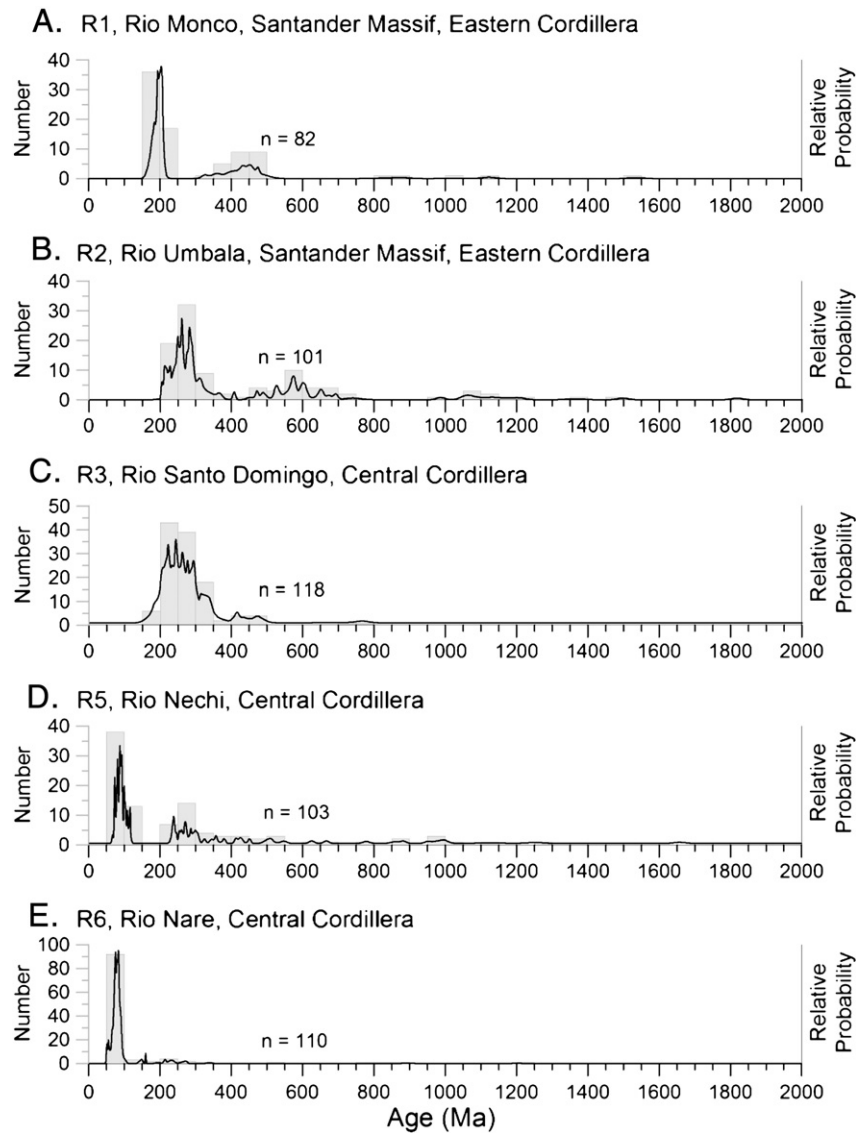
Fig. 5. Detrital zircon U–Pb age spectra of five modern river samples from regions bordering the Middle Magdalena Valley basin (Fig. 1A). Age spectra are depicted as age probability functions (thick lines) and age histograms (gray bars). Note that scale of age probability function curves has been adjusted to fit the figure and thus area under the age probability function curves is not equal for each sample.

of In, Cs, Re, and Bi. The trace element concentrations were obtained using known U.S. Geological Survey standards BCR-2 and BIR-2. The reported concentrations of trace elements have 2–5% uncertainties on the basis of repeated measurements of SRM-278 (Obsidian-NIST) and BHVO (USGS-Basalt) standards.

Nd isotopes were measured using chemical and mass spectrometric procedures at the University of Rochester (Basu et al., 1990). Measured $^{143}Nd/^{144}Nd$ ratios were normalized to $^{146}Nd/^{144}Nd = 0.7219$. The La Jolla Nd standard analyzed during the course of this study yielded $^{143}Nd/^{144}Nd = 0.511853 \pm 0.000034$ (2σ, n = 5) and εNd (t = 0) values were calculated using the present-day bulk Earth value of $^{143}Nd/^{144}Nd = 0.512638$. Depleted mantle model ages (T_{DM}) were estimated assuming a linear growth in εNd values of depleted mantle from εNd = 0 at 4.56 Ga to a present-day depleted mantle value of εNd = 10 by using $^{147}Sm/^{144}Nd = 0.2136$ (Table 1).

6.4. Sandstone petrography

6.4.1. Rationale

Acquisition of sandstone compositional data from point-counting (systematic identification and classification of constituent minerals

and lithic fragments) yields quantitative information on contributing source lithologies. Samples are categorized by sandstone type or tectonic setting based on the proportions of characteristic minerals or lithic grains such as quartz, feldspar, or sedimentary, volcanic, and metamorphic fragments (Dickinson and Suczek, 1979; Folk, 1980; Dickinson et al., 1983; Ingersoll et al., 1984).

Though sandstone compositions are primarily a function of a basin's tectonic setting (Dickinson and Suczek, 1979; Ingersoll et al., 1984), factors other than source region can affect sandstone composition. For example, intense chemical weathering and diagenesis can also affect the composition of sandstone, notably through the preferential breakdown of unstable feldspar and lithic grains (Suttner et al., 1981; Suttner and Basu, 1985; Milliken, 1988).

6.4.2. Methods

A total of 65 thin sections were counted according to the Gazzi–Dickinson method, in which the constituent mineral directly under the cross-hairs of the petrographic microscope is identified and counted (Gazzi, 1966; Dickinson, 1970; Ingersoll et al., 1984). For each sample, 450 framework sand grains were counted and categorized (Moreno et al., 2011). Thin sections were stained for plagioclase

Table 1
Sm–Nd isotopic data of the Middle Magdalena Valley basin. Note: Tdm were calculated using the model of DePaolo (1981). $\varepsilon Nd(0) = \{[(^{143}Nd/^{144}Nd)sample/(^{143}Nd/^{144}Nd)CHUR] - 1\} \times 10^4$, where $(^{143}Nd/^{144}Nd)_{CHUR} = 0.512638$.

Sample ID	Sm (ppm)	Nd (ppm)	^{147}Sm	^{144}Nd	$^{147}Sm/^{144}Nd$	$^{143}Nd/^{144}Nd$	$\varepsilon Nd(0)$	Tdm (Gyr)
N1	6.8655139	35.4439002	1.0346329	8.1627302	0.1268	0.511931	−13.8	2.13
N2	4.8386297	26.9606200	0.7291815	6.2090308	0.1174	0.512040	−11.7	1.76
N3	6.6268189	38.3763398	0.9986616	8.8380710	0.1130	0.512174	−9.1	1.48
N4	1.9095595	11.3435758	0.2877706	2.6124255	0.1102	0.511947	−13.5	1.77
N5	3.6006525	23.0987966	0.5426183	5.3196528	0.1020	0.511823	−15.9	1.81
N6	5.1096901	27.1600768	0.7700303	6.2549657	0.1231	0.511944	−13.5	2.02
N7	3.8676672	18.1633014	0.5828574	4.1830083	0.1393	0.511934	−13.7	2.48
N8	5.2189233	27.8687851	0.7864917	6.4181812	0.1225	0.511913	−14.1	2.06

(P) and potassium feldspar (K). Raw data were parameterized for each sample and calculated as total quartz [Q = monocrystalline quartz (Qm) + polycrystalline quartz (Qp) + polycrystalline quartz with tectonic fabric (Qpt) + chert lithic fragments (Lch)], feldspar [F = plagioclase (P) + potassium feldspar (K)], and lithic fragments of sedimentary (Ls), volcanic (Lv), and metamorphic (Lm) rocks.

7. Results

7.1. Detrital zircon U–Pb geochronology

7.1.1. River sand samples

Detrital zircon U–Pb ages for unconsolidated sand samples from five modern rivers (Fig. 1) reveal distinctions between CC and EC sources (Fig. 5). EC samples R1 and R2 represent rivers draining the northernmost EC (Santander basement massif). EC sample R1 (Rio Manco) yields a U–Pb age spectrum dominated by ages between 240 and 150 Ma with additional ages distributed between 500 and 300 Ma. EC sample R2 (Rio Umbala) is dominated by ages between 350 and 200 Ma; additional ages are distributed at 700–450 Ma and 1100–1050 Ma. CC samples R3–R5 are from rivers draining the northernmost CC and San Lucas range. CC sample R3 (Rio Santo Domingo) is dominated by ages between 350 and 180 Ma; additional ages are distributed between 500 and 400 Ma. CC sample R5 (Rio Nechi) is dominated by 120–75 Ma ages with a peak age of 90 Ma. In addition, ages of 320–230, 410, 450, and 510 Ma also represent significant subpopulations (defined by three or more grains). CC sample R6 (Rio Nare) is dominated by one major peak at 84 Ma, with minor peaks at 145–160 Ma and 200–255 Ma. Based on these results, it is clear that U–Pb ages younger than 150 Ma come from the CC rather than the EC (Tables DR1 and DR2) (Fig. 5). However, one EC river (R2) has a Grenville component (1100–1050 Ma) not present in CC rivers.

7.1.2. Sandstone samples

U–Pb ages from most of the 13 sandstone samples (Fig. 4), excluding Z5–Z9, have been published previously (Nie et al., 2010) (Table DR1). U–Pb age spectra reveal two Cenozoic shifts in provenance (Nie et al., 2010). The first shift occurs between lower and upper Paleocene strata, where U–Pb results show a switch from Proterozoic-dominated to Phanerozoic-dominated age spectra (Fig. 4). The second shift occurs between middle–upper Eocene and upper Oligocene strata, where increased proportions of Grenville-age zircons are accompanied by a reduction in Mesozoic-age zircons (Fig. 4). The new age data presented here for samples Z5–Z9 (Fig. 4; Table DR2), which span the upper La Paz to upper Esmeraldas formations, place a tighter age constraint (middle–upper Eocene) on the second provenance shift (between lower and middle Esmeraldas).

The basal Esmeraldas sample (Z5) is dominated by a 300–100 Ma age population with no Mesoproterozoic Grenville-age component; in contrast, samples Z6–Z9 all have Grenville signatures at 1200–900 Ma. The middle Esmeraldas sample (Z6) also has significant age peaks at 280, 200, and 80 Ma. The upper Esmeraldas sample

(Z7) has significant age peaks at 260 and 75 Ma. The lower Mugrosa sample (Z8) has significant age peaks at 465, 435, and 205 Ma. The middle Mugrosa sample (Z9) has significant age peaks at 440, 245, 215, and 185 Ma.

We attribute the mid-Paleocene change between the lower and upper Lisama Formation to uplift-induced exhumation of the CC signaled by the appearance of 150–100 Ma detrital zircon U–Pb ages in the upper Lisama Formation (Fig. 4). This reflects an age group for CC basement distinct from that of the Guyana shield (Amazonian craton) and EC basement (Fig. 5). East-directed paleocurrents in the upper Lisama Formation support this conclusion (Moreno et al., 2011). We link the second shift in U–Pb age spectra between middle–upper Eocene and upper Oligocene strata to exhumation of the EC based on the increased amount of Grenville ages and diminished proportion of Mesozoic ages (Fig. 4). According to the results of five additional samples presented here, the appearance of Grenville ages can be further pinpointed between the lower and middle Esmeraldas Formation (Fig. 4), indicating earliest detrital evidence of major exhumation of the EC between the middle and late Eocene. This conclusion is consistent with west-directed paleocurrents for the middle to upper Esmeraldas Formation (Caballero et al., 2010). Late Cretaceous zircon ages do not disappear until the lower Mugrosa Formation (Fig. 4), suggesting possible recycling of the uppermost EC sedimentary cover, specifically the upper Paleocene–middle Eocene section originally derived from the CC.

7.2. Heavy mineral analysis

7.2.1. River sand samples

Modern river samples from the CC and EC are dominated by hornblende and epidote, but each carries distinctive heavy mineral signatures (Fig. 6) (Table DR3). Sample R1 (Rio Monco) is unique with its dark green chloritoid and fairly high garnet content. R3 (Rio Santo Domingo) has the highest proportion of epidote-group minerals and garnet. R5 (Rio Nechi) is distinguished by high proportions of
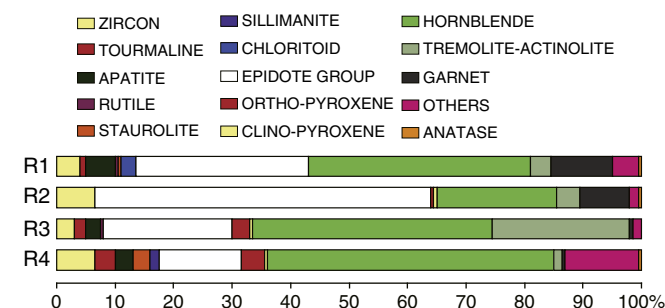

Fig. 6. Heavy mineral assemblages of four modern river samples from regions bordering the Middle Magdalena Valley basin (Fig. 1A).

tremolite-actinolite. R4 (Rio Swan) is characterized by abundant an-
dalusite and a small amount of staurolite.

7.2.2. Sandstone samples

Heavy minerals and varieties of zircon and tourmaline grains in
the sandstone samples are plotted as bar charts (Figs. 4 and 7) (Tables
DR3 and DR4). Similar to heavy mineral distributions from Venezuela
and Trinidad (Pindell et al., 2009), the sandstones in Colombia are
rich in zircon and tourmaline, probably related to intense chemical
weathering and elimination of less-stable minerals have been partial-
ly or completely eliminated. Nevertheless, compositional variations of
heavy minerals and morphological variations of more-stable minerals
prove to be reliable proxies for provenance changes.

Two samples from the Maastrichtian Umir Formation contain
strikingly different heavy mineral compositions (Fig. 4). The low di-
versity of the lower Umir Formation sample (H1) contrasts with the
varied assemblages of the upper Umir sample (H2). Whereas garnet
and chloritoid (associated with epidote and a few serpentine grains)
are important in sample H2, they are not observed in H1. H2 contains
the highest percentage of apatite for the entire sample set. Garnet,
chloritoid and serpentine minerals may originate from a relict meta-
ophiolitic and/or chloritoid-bearing high-pressure complex. The pro-
portions of euhedral zircon and sharp prismatic tourmaline do not
show an increase from the lower to upper Umir Formation, and
rounded grains dominate zircon and tourmaline morphology
(Fig. 7). These observations suggest that materials from the Umir For-
mation likely experienced multiple episodes of recycling, consistent
with a cratonic provenance.

Assemblages of the Paleocene Lisama Formation (Fig. 4) display a
shift from the zircon- and tourmaline-dominated lower Lisama (sam-
ple H3) to the more diverse upper Lisama (sample H4). Staurolite
grains first appear in upper Lisama strata and remain present in over-
lying units. The appearance of staurolite in H4 signals the emergence
of metamorphic basement lithologies. Accompanying this change, the
proportion of euhedral zircon increases (Fig. 7). These observations
argue for a provenance shift from an eastern craton source to the
metamorphic foundation of the CC in the west. Similarly, the corre-
sponding appearance of <200 Ma zircon U–Pb ages also suggests ex-
humation of the CC.

There is a marked mineralogical difference between the lower,
middle, and upper levels of the lower–middle Eocene La Paz

Formation (Fig. 4). The lower La Paz sample (H5) is dominated by zir-
con, tourmaline, and rutile associated with staurolite, epidote, and
anatase. The middle La Paz sample (H6) has more diverse mineral as-
semblages, characterized by the abundance of zircon, tourmaline, ru-
tile, garnet, dark green chloritoid, and traces of andalusite. Zircon
varieties show greater angularity and euhedral crystals. Such signa-
tures define a prominent reorganization of the source provinces
and/or transport from newly exhumed lithologies. Lower diversity
suites return in the upper La Paz sample (H7), which contains high
proportions of euhedral zircons and sharp prismatic tourmalines indi-
cating continued first-cycle input (Fig. 7). We attribute the introduc-
tion of chloritoid and highest proportion of euhedral zircons in
lower–middle Eocene La Paz strata to exposure of the MMVB base-
ment paleohigh, which was subsequently buried by upper Eocene
strata (Gómez et al., 2005). Overall, a higher proportion of euhedral
zircons and decreased roundness of zircon and tourmaline grains in
the La Paz Formation relative to underlying formations support a con-
tinued basement source, probably from the CC and MMVB basement
paleohigh.

The upper Eocene–lower Oligocene Esmeraldas Formation is
enriched in highly stable minerals and contains limited staurolite
(Fig. 4). Abundant degraded biotite is present in the lower Esmeral-
das (sample H8). There is a marked upsection decrease in euhedral
zircons and increase in rounded tourmalines from the lower to
upper Esmeraldas (sample H9) (Fig. 7). These changes indicate a de-
creased contribution from basement exhumation and an increased
contribution from sedimentary recycling. This record is consistent
with zircon U–Pb results, which suggest the initiation of exhumation
in the EC, which was covered by sediments originally derived from
the CC and/or Guyana shield. Erosional stripping of this sedimentary
cover accounts for the introduction of increased amounts of recycled
zircon and tourmaline grains.

Heavy mineral compositions for the Oligocene Mugrosa Formation
(samples H10 and H11) are similar to that of the upper Esmeraldas
(H9), suggesting continued recycling of the sediment cover in the
growing EC fold–thrust belt.

In summary, the sandstone samples are generally dominated by
zircon and tourmaline with subordinate rutile. Of the provenance-
diagnostic minerals, staurolite first appears in the upper Lisama For-
mation and remains in the overlying La Paz, Esmeraldas and Mugrosa
formations. We attribute the appearance of staurolite to exhumation
of the CC, a region floored by a Paleozoic metamorphic belt. The La
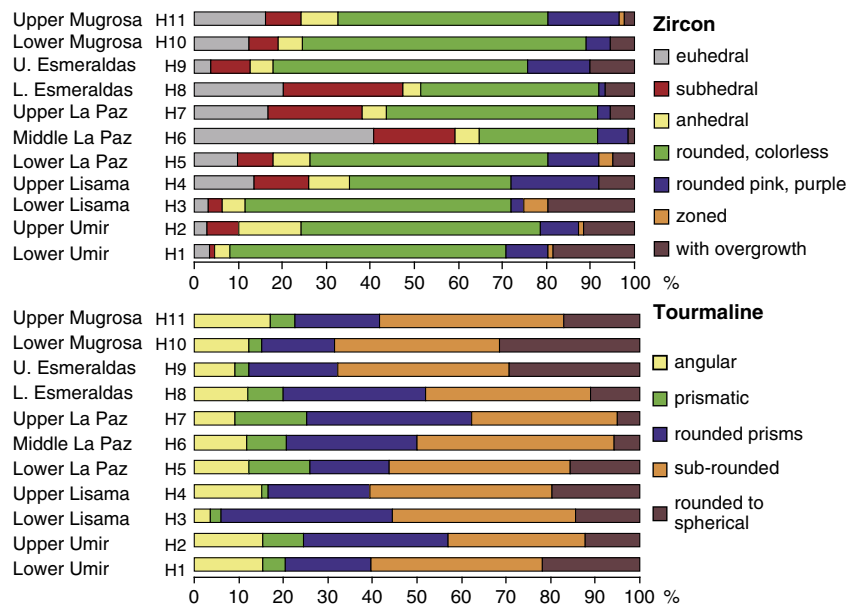

Fig. 7. Grain morphology variations for zircon and tourmaline grains of eleven sandstone samples from the Middle Magdalena Valley basin (H1–H11 in Fig. 3).

Paz Formation is enriched in tourmaline, whereas zircon occurs in much lower proportions. From the high proportions of euhedral zircons and sharp prismatic tourmalines, it is evident that the La Paz contains the highest amount of first-cycle input from the CC and the MMVB basement paleohigh. Proportions of zircons decrease and rounded tourmalines increase from the lower to upper Esmeraldas Formation, signifying reduced first-cycle input and another provenance shift. We attribute this shift to shortening-related exhumation in the EC fold–thrust belt which induced recycling of the EC sedimentary cover and the observed decrease in first-cycle input. Upsection within the Mugrosa Formation, diminished amounts of zircons and increased proportions of rounded tourmalines indicate continued recycling of the EC sedimentary cover during further exhumation of the fold–thrust belt.

7.3. Nd isotope analysis

Mudstone samples analyzed for Nd isotopic values exhibit internally similar chondrite-normalized REE distribution patterns similar to post-Archean shales from Australia (PAAS) (Taylor and McLennan, 1985) (Fig. 8). Sample N7 has a positive Ce anomaly (Fig. 8), probably caused by the presence of a phosphate mineral and/or zircon.

$\varepsilon_{Nd(t=0)}$ values show an increase in isotopic values from the lower Lisama (-13.8) to upper Lisama and then lower La Paz Formation (Fig. 4). Upsection, $\varepsilon_{Nd(t=0)}$ values decrease from the lower La Paz to the lower Esmeraldas Formation (Fig. 4). Strata overlying the lower Esmeraldas Formation have relatively constant $\varepsilon_{Nd(t=0)}$ values of ~-14.

A trend towards more positive $\varepsilon_{Nd(t=0)}$ values from the upper Lisama to lower La Paz indicates a transition from older (more evolved) to more juvenile sources for fine-grained sediments, consistent with evidence from zircon U–Pb ages and heavy mineral data for initial exhumation of the CC. In contrast, more negative $\varepsilon_{Nd(t=0)}$ values from the upper La Paz to lower Esmeraldas appear to contradict zircon U–Pb ages, which continue to be dominated by relatively youthful Phanerozoic ages, suggesting little contribution from the more negative $\varepsilon_{Nd(t=0)}$ rocks of the more evolved eastern craton. Further, a consistent western source for the lower La Paz to lower Esmeraldas is supported by eastward paleocurrents, a higher proportion of euhedral zircons, a reduced amount of rounded tourmalines (H5, H6, H7, and H8 in Fig. 7). However, an intriguing pattern is revealed in which chloritoid briefly appears in the middle La Paz Formation (middle Eocene) and then disappears in the upper La Paz Formation (middle–late Eocene) (Fig. 4). The stratigraphic appearance and disappearance of chloritoid may signify exhumation and then burial of the La Cira–Infantas basement paleohigh, presently buried beneath upper Eocene–Quaternary basin fill of the MMVB along the western flank of the Nuevo Mundo syncline (Gómez et al., 2005). We propose

that uplift of the MMVB basement paleohigh can explain the contradiction of increased first-cycle Phanerozoic-age zircons yet more negative $\varepsilon_{Nd(t=0)}$ values (<-14). This explanation requires that the MMVB basement paleohigh consists of old, highly evolved continental crust with more negative $\varepsilon_{Nd(t=0)}$ values.

For stratigraphic units overlying the Esmeraldas Formation, $\varepsilon_{Nd(t=0)}$ values increase to consistent values near -14. This observation can be explained by protracted recycling of the originally craton-derived Mesozoic sedimentary cover from uplifted regions of the EC fold–thrust belt.

7.4. Sandstone petrography

Although intensive chemical weathering in the tropical regions of Colombia ensures that nearly all sandstone samples are dominated by quartz, several stratigraphic trends in sandstone composition are present (Fig. 4D). Because quartz (Q) is ubiquitous, the following description focuses on variations with the lithic fraction. In the lowest sample from the lower Lisama Formation, feldspar (F) combined with lithic metamorphic (Lm), volcanic (Lv), and sedimentary (Ls) fragments compose 31% of the framework grains. Both Lm and Lv increase from lower to upper levels of the Lisama Formation, reaching maximum values of ~17% and ~22%, respectively, at the Lisama–La Paz contact. The percentage of Lv grains and, to a lesser extent, Lm grains remains high throughout the lower La Paz Formation. The percentage of Lv grains decreases from the lower to upper La Paz (Fig. 4D). In contrast, the percentages of F, Ls, and Lm grains remain unchanged throughout the La Paz Formation. F, Lv, and Lm percentages for the lower La Paz are ~5%, ~11%, and ~9%, respectively, and ~2%, ~1%, and ~5%, respectively for the upper La Paz and Esmeraldas formations. The lithic composition of the overlying Mugrosa Formation is uniformly low. However, lithic components farther upsection again compose significant fractions of sandstones in the Colorado and Real formations.

The increase in Lv from the lower to upper Lisama Formation is consistent with a provenance shift from the eastern craton to the CC, reinforcing the aforementioned interpretation from other provenance proxies. From the lower to upper La Paz Formation, the decrease in Lv likely derived from the CC magmatic arc roughly coincides with more negative $\varepsilon_{Nd(t=0)}$ values and the appearance of garnet and chloritoid. These variations are consistent with exhumation of the La Cira–Infantas basement paleohigh, a complex feature now buried beneath upper Eocene–Quaternary fill of the MMVB along the western flank of the Nuevo Mundo syncline. Although Nd isotope and zircon U–Pb ages all detect a provenance shift from the lower to middle Esmeraldas Formation associated with exhumation of the EC, no significant change is observed in sandstone compositions. This consistency in sandstone compositions potentially indicates compositional similarity between rocks uplifted by the MMVB (La Cira–Infantas) basement structures in the west and the EC in the east (Moreno et al., 2011).

8. Discussion

The integrated provenance techniques employed here reveal a series of significant shifts in the geochronology, mineralogy, and geochemistry of detrital sediments in the MMVB. Uppermost Cretaceous to Neogene fill of the MMVB recorded a series of shifts: from (1) exclusively cratonic to (2) magmatic arc, then (3) combined arc and uplifted continental block, and finally (4) retroarc fold–thrust belt (Fig. 9).

First, a cratonic source is indicated for the Maastrichtian Umir Formation and lower Paleocene levels of the Lisama Formation. Precambrian U–Pb ages for detrital zircon grains, more negative $\varepsilon_{Nd(t=0)}$ values, lower Lv proportions, and lower euhedral zircon content (Figs. 4, 7, and 9A) support this argument. Available paleocurrent
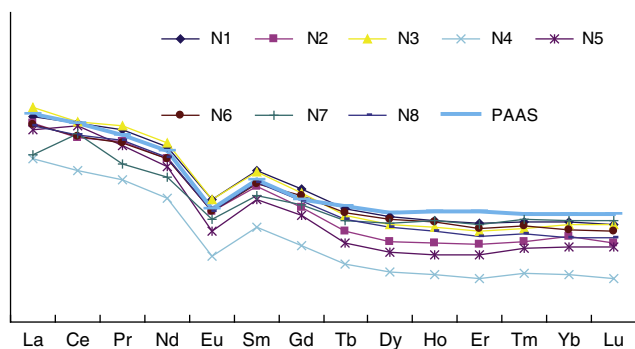

Fig. 8. Chondrite-normalized rare earth element (REE) distribution of sandstone samples from the Middle Magdalena Valley basin (N1–N8 in Fig. 3) and their comparison with post-Archean shales from Australia (PAAS).
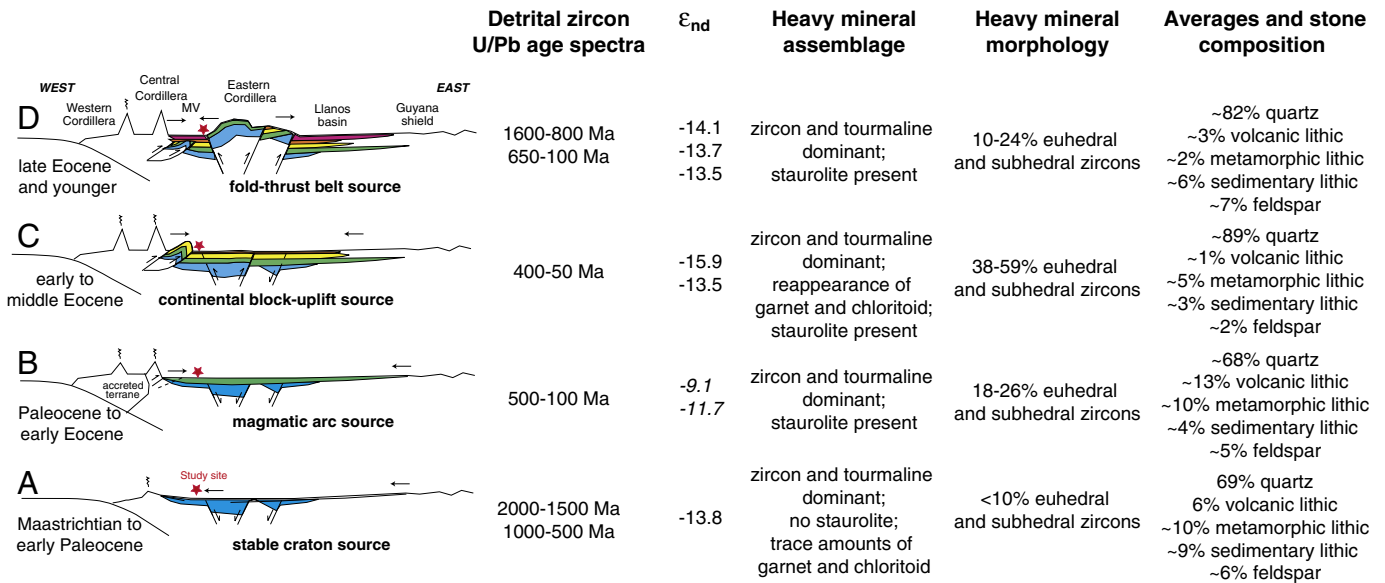
	Detrital zircon U/Pb age spectra	ε_{nd}	Heavy mineral assemblage	Heavy mineral morphology	Averages and stone composition
D late Eocene and younger — **fold-thrust belt source**	1600-800 Ma 650-100 Ma	-14.1 -13.7 -13.5	zircon and tourmaline dominant; staurolite present	10-24% euhedral and subhedral zircons	~82% quartz ~3% volcanic lithic ~2% metamorphic lithic ~6% sedimentary lithic ~7% feldspar
C early to middle Eocene — **continental block-uplift source**	400-50 Ma	-15.9 -13.5	zircon and tourmaline dominant; reappearance of garnet and chloritoid; staurolite present	38-59% euhedral and subhedral zircons	~89% quartz ~1% volcanic lithic ~5% metamorphic lithic ~3% sedimentary lithic ~2% feldspar
B Paleocene to early Eocene — **magmatic arc source**	500-100 Ma	-9.1 -11.7	zircon and tourmaline dominant; staurolite present	18-26% euhedral and subhedral zircons	~68% quartz ~13% volcanic lithic ~10% metamorphic lithic ~4% sedimentary lithic ~5% feldspar
A Maastrichtian to early Paleocene — **stable craton source**	2000-1500 Ma 1000-500 Ma	-13.8	zircon and tourmaline dominant; no staurolite; trace amounts of garnet and chloritoid	<10% euhedral and subhedral zircons	69% quartz 6% volcanic lithic ~10% metamorphic lithic ~9% sedimentary lithic ~6% feldspar

Fig. 9. Reconstruction of uppermost Cretaceous–Cenozoic geologic history (after Horton et al., 2010b) and corresponding provenance signatures for different sediment sources, arranged in stratigraphic order. (A) Stable craton; (B) magmatic arc; (C) continental block-uplift; and (D) fold–thrust belt.

data indicate northward flow for the lower Lisama Formation in the MMVB (Moreno et al., 2011) and west/northwestward flow across the EC and Llanos basin (Cooper et al., 1995) during the latest Cretaceous–early Paleocene, consistent with a cratonic source.

Second, a mid-Paleocene change in the middle Lisama Formation is revealed by the appearance of Phanerozoic ages in detrital zircon U–Pb age spectra, increased euhedral zircon and sharp prismatic tourmaline, appearance of staurolite in heavy mineral assemblages, shift to eastward paleocurrents, and increased $\varepsilon_{Nd(t=0)}$ values (Figs. 4, 7, and 9B). Although many authors argue that the initiation of CC uplift occurred earlier, during the Late Cretaceous, there is no evidence for a wholesale shift in provenance at that time. Assessment of recent fission track results from the CC reveals that, excluding a few ages with large uncertainties, the Late Cretaceous fission track ages correspond to igneous rocks (Villagómez, 2010) and may reflect the age of Cretaceous magmatic cooling rather than cooling associated with exhumation. Therefore, we maintain that initial shortening-related rock uplift and exhumation of the CC did not occur until mid-Paleocene time.

Third, an early–middle Eocene provenance change in the middle La Paz Formation is revealed by a shift to more negative $\varepsilon_{Nd(t=0)}$ values, to higher Q and lower Lv content, to higher amounts of euhedral and subhedral zircons, and the reappearance of garnet and chloritoid grains (Figs. 4, 7, and 9C). Considering the east-directed paleocurrents for the La Paz (Moreno et al., 2011) and the subsurface MMVB unconformity (with basement overlapped by undeformed middle Eocene to Neogene strata; Gómez et al., 2005), we attribute the provenance change to uplift of the MMVB basement paleohigh.

Fourth, zircon U–Pb age data suggest that major exhumation of the EC commenced during the middle–late Eocene between deposition of the lower and middle Esmeraldas Formation (Fig. 4 and 9D). This interpretation is supported by a decreased proportion of euhedral crystals, increased amount of rounded tourmaline grains, and upsection switch from east- to west-directed paleocurrents. However, there is no distinct difference in terms of heavy mineral compositions, suggesting that grain morphology can be a useful attribute in tropical areas such as the northern Andes. An increase in the $\varepsilon_{Nd(t=0)}$ values from the lower to upper Esmeraldas signifies rock uplift of the EC, which probably exhibits less negative $\varepsilon_{Nd(t=0)}$ values in comparison to the MMVB basement.

Several potential complexities affecting provenance techniques need to be considered. In terms of climate, large spatial gradients in precipitation across Colombia have existed only since 6–3 Ma, when surface uplift of the EC reached threshold elevations sufficient for the generation of a rain shadow on the leeward (western) side of the EC (Mora et al., 2008). Moreover, northwestern South America has resided consistently at tropical latitudes since ~70 Ma (Zachos et al., 2001). These factors suggest that spatial variations in climate were unlikely to alter provenance proxies during latest Cretaceous to Miocene evolution of the MMVB. Any temporal changes in climate, such as glacial expansion events during the early Oligocene and early Miocene (Zachos et al., 2001), would have had relatively uniform effects on the principal source regions (WC, CC, EC, craton) of Colombia.

Potential problems related to sediment recycling and nonunique source regions can also be addressed for Colombia. As the clearest example, Grenville-age (1200–900 Ma) zircons are present not only in the craton (Guyana shield) but also in EC crystalline basement, Cretaceous basin fill of the EC, and probably at depth in the MMVB basement paleohigh (Restrepo-Pace et al., 1997; Horton et al., 2010b). Nevertheless, diagnostic paleocurrent patterns combined with the presence or absence of key detrital signatures (such as F- and Lv-rich sandstone compositions and Mesozoic zircon ages from magmatic-arc rocks of the WC) allow for estimation of the switch from cratonic to Andean sediment sources and the relative timing of major exhumation in the CC, EC, and MMVB. This tectonic history includes the complex recycling of Mesozoic sedimentary rocks originally derived from eastern cratonic sources (including Grenville-age signatures) that were subsequently re-exhumed during uplift of the EC and redistributed westward to the MMVB (Nie et al., 2010; this study) and eastward to the Llanos foreland (Horton et al., 2010a).

Application of multiple provenance techniques provides a relatively high-resolution history of the tectonic evolution of the MMVB. Unlike techniques applied individually, an integrated approach is less affected by complicating factors such as chemical weathering and sediment recycling. In this study, we are able to detect not only the major shifts but also short-term pulses, such as the brief exposure of MMVB basement. The use of multiple provenance proxies provides the ability to both detect provenance changes and characterize evolving source areas based on differences in mineralogy, age, and geochemistry.

9. Conclusions

The integrated provenance techniques employed here for the northern Andes of Colombia reveal a series of significant shifts in the geochronology, paleocurrents, mineralogy, and geochemistry of detrital sediments in the uppermost Cretaceous to Neogene strata of the MMVB. These diverse approaches reveal changes in principal source regions from (1) exclusively cratonic (latest Cretaceous–early Paleocene) to (2) magmatic arc (late Paleocene–early Eocene), then (3) combined arc and uplifted continental block (early–middle Eocene), and finally (4) retroarc fold–thrust belt (late Eocene–Miocene). The change from a craton (Precambrian Guyana shield) to magmatic arc (Mesozoic CC) source is characterized by introduction of relatively youthful Phanerozoic-age detrital zircons, higher (more juvenile) $\varepsilon_{Nd(t=0)}$ values, introduction of staurolite in the heavy mineral assemblages, an increase in Lv sand grains, and a change to eastward paleocurrents. With uplift of the MMVB basement, there is little change in the detrital zircon U–Pb age distributions, a decrease in $\varepsilon_{Nd(t=0)}$ values, the short-lived appearance of garnet in the heavy mineral assemblages coupled with an increase in euhedral resistant minerals, an increase in quartz at the expense of all lithic sand grains, and no major change in paleocurrents. Initial exhumation of the EC fold–thrust belt in the late Eocene resulted in re-introduction of abundant Proterozoic-age zircons, little change in the $\varepsilon_{Nd(t=0)}$ values, increased roundness of resistant minerals, the disappearance of Lm and Lv sand grains, and a change to westward paleocurrents. The relatively high fidelity of the provenance signal in the MMVB, despite the intense humid climate and protracted sedimentary recycling, may be the product of both the diversity of potential sources and the relatively short transport distances (typically < 200–500 km) from source to sink.

In this study, application of multiple provenance techniques has proven essential both in identifying provenance shifts and in characterizing source regions. Integrated studies utilizing multiple provenance techniques may be particularly suitable for convergent retroarc systems where competing sources include the stable craton, magmatic arc, and recycled sedimentary rocks (and local basement) of the fold–thrust belt. As exemplified in this study, recycling of sediments, extreme climate conditions, nonunique sources, and heterogeneous sources need not render a provenance study invalid. Rather, construction of hypotheses recognizing the high probability of sediment recycling and variability in climate and sediment sources are apt to define more robust reconstructions of the temporal and spatial evolution of uplifted sediment source regions. Similar studies utilizing multiple provenance techniques may be further suited for cases requiring discrimination between similar sediment sources or cases where provenance signals are obscured by recycling, chemical weathering, or other modifications during and after transport and deposition.

Supplementary materials related to this article can be found online at doi:10.1016/j.earscirev.2011.11.002.

References

Allen, P.A., 2008. From landscapes into geological history. Nature 451 (7176), 274–276.

Amano, K., Taira, A., 1992. Two-phase uplift of higher Himalayas since 17 Ma. Geology 20 (5), 391–394.

Amidon, W.H., Burbank, D.W., Gehrels, G.E., 2005a. Construction of detrital mineral populations: insights from mixing of U–Pb zircon ages in Himalayan rivers. Basin Research 17 (4), 463–485.

Amidon, W.H., Burbank, D.W., Gehrels, G.E., 2005b. U–Pb zircon ages as a sediment mixing tracer in the Nepal Himalaya. Earth and Planetary Science Letters 235 (1–2), 244–260.

Aspden, J.A., McCourt, W.J., 1986. Mesozoic oceanic terrane in the central Andes of Colombia. Geology 14 (5), 415–418.

Aspden, J.A., McCourt, W.J., Brook, M., 1987. Geometrical control of subduction-related magmatism—the Mesozoic and Cenozoic plutonic history of western Colombia. Journal of the Geological Society 144, 893–905.

Basu, A.R., Sharma, M., DeCelles, P.G., 1990. Nd, Sr-isotopic Nd, Sr-isotopic provenance and trace element geochemistry of Amazonian foreland basin fluvial sands, Bolivia and Peru: implications for ensialic Andean orogeny. Earth and Planetary Science Letters 100 (1–3), 1–17.

Bayona, G., Cortés, M., Jaramillo, C., Ojeda, G., Aristizabal, J.J., Reyes-Harker, A., 2008. An integrated analysis of an orogen–sedimentary basin pair: Latest Cretaceous–Cenozoic evolution of the linked Eastern Cordillera orogen and the Llanos foreland basin of Colombia. Geological Society of America Bulletin 120, 1171–1197.

Bernet, M., Zattin, M., Garver, J.I., Brandon, M.T., Vance, J.A., 2001. Steady-state exhumation of the European Alps. Geology 29 (1), 35–38.

Caballero, V., Parra, M., Mora, A., 2010. Levantamiento de la Cordillera Oriental de Colombia durante el Eoceno tardió–Oligoceno temprano: Proveniencia sedimentaria en el sinclinal de Nuevo Mundo, cuenca Valle Medio del Magdalena. Boletín de Geologia 32, 45–77.

Carrapa, B., DeCelles, P.G., Reiners, P.W., Gehrels, G.E., Sudo, M., 2009. Apatite triple dating and white mica $^{40}Ar/^{39}Ar$ thermochronology of syntectonic detritus in the Central Andes: a multiphase tectonothermal history. Geology 37 (5), 407–410.

Carroll, A.R., Graham, S.A., Hendrix, M.S., Ying, D., Zhou, D., 1995. Late Paleozoic tectonic amalgamation of Northwestern China—sedimentary record of the northern Tarim, northwestern Turpan, and southern Junggar basins. Geological Society of America Bulletin 107 (5), 571–594.

Chang, Z.S., Vervoort, J.D., McClelland, W.C., Knaack, C., 2006. U–Pb dating of zircon by LA–ICP-MS. Geochemistry, Geophysics, Geosystems 7, Q05009. doi:10.1029/2005GC001100.

Chew, D.M., Schaltegger, U., Košler, J., Whitehouse, M.J., Gutjahr, M., Spikings, R.A., Mišković, A., 2007. U–Pb geochronologic evidence for the evolution of the Gondwanan margin of the north-central Andes. Geological Society of America Bulletin 119 (5–6), 697–711.

Chew, D.M., Magna, T., Kirkland, C.L., Miskovic, A., Cardona, A., Spikings, R., Schaltegger, U., 2008. Detrital zircon fingerprint of the Proto-Andes: evidence for a Neoproterozoic active margin? Precambrian Research 167 (1–2), 186–200.

Condie, K.C., 1998. Episodic continental growth and supercontinents: a mantle avalanche connection? Earth and Planetary Science Letters 163 (1–4), 97–108.

Cooper, M.A., Addison, F.T., Alvarez, R., Coral, M., Graham, R.H., Hayward, A.B., Howe, S., Martinez, J., Naar, J., Penas, R., Pulham, A.J., Taborda, A., 1995. Basin development and tectonic history of the Llanos Basin, Eastern Cordillera, and middle Magdalena Valley, Colombia. American Association of Petroleum Geologists Bulletin 79 (10), 1421–1443.

Copeland, P., Harrison, T.M., 1990. Episodic rapid uplift in the Himalaya revealed by $^{40}Ar/^{39}Ar$ analysis of detrital K-Feldspar and muscovite, Bengal fan. Geology 18 (4), 354–357.

Cordani, U.G., Sato, K., Teixeira, W., Tassinari, C.G., Basei, M.A.S., 2000. Tectonic evolution of South America. In: Cordani, U.G., Milani, E.J., Thomaz Filho, A., Campos Neto, M.C. (Eds.), 31st International Geological Congress. Recherche pour le Développement, Rio de Janeiro, pp. 19–40.

Cowan, D.S., Brandon, M.T., Garver, J.I., 1997. Geologic tests of hypotheses for large coastwise displacements—a critique illustrated by the Baja British Columbia controversy. American Journal of Science 297 (2), 117–173.

Cox, R., Lowe, D.R., 1995. A conceptual review of regional-scale controls on the composition of clastic sediment and the co-evolution of continental blocks and their sedimentary cover. Journal of Sedimentary Research 65 (1), 1–12.

Cox, R., Lowe, D.R., Cullers, R.L., 1995. The influence of sediment recycling and basement composition on evolution of Mudrock chemistry in the southwestern United-States. Geochimica et Cosmochimica Acta 59 (14), 2919–2940.

Cullers, R.L., Basu, A., Suttner, L.J., 1988. Geochemical signature of provenance in sand-size material in soils and stream sediments near the Tobacco Root Batholith, Montana, USA. Chemical Geology 70 (4), 335–348.

Davis, D.W., Lin, S.F., 2003. Unraveling the geologic history of the Hemlo Archean gold deposit, Superior province, Canada: a U–Pb geochronological study. Economic Geology and the Bulletin of the Society of Economic Geologists 98 (1), 51–67.

Davis, D.W., Williams, I.S., Krogh, T.E., 2003. Historical development of zircon geochronology. In: Hanchar, J.M., Hoskin, P.W.O. (Eds.), Zircon: Reviews in Mineralogy & Geochemistry, pp. 145–181.

DeCelles, P.G., 1988. Lithologic provenance modeling applied to the Late Cretaceous synorogenic Echo Canyon Conglomerate, Utah: a case of multiple source areas. Geology 16 (11), 1039–1043.

DeCelles, P.G., Gehrels, G.E., Quade, J., Ojha, T.P., Kapp, P.A., Upreti, B.N., 1998. Neogene foreland basin deposits, erosional unroofing, and the kinematic history of the Himalayan fold–thrust belt, western Nepal. Geological Society of America Bulletin 110 (1), 2–21.

DeCelles, P.G., Gehrels, G.E., Quade, J., LaReau, B., Spurlin, M., 2000. Tectonic implications of U–Pb zircon ages of the Himalayan orogenic belt in Nepal. Science 288 (5465), 497–499.

Dengo, C.A., Covey, M.C., 1993. Structure of the Eastern Cordillera of Colombia; implications for trap styles and regional tectonics. AAPG Bulletin 77 (8), 1315–1337.

DePaolo, D.J., 1981. Neodymium isotopes in the Colorado front range and crust–mantle evolution. Nature 291, 193–196.

Derry, L.A., France-Lanord, C., 1996. Neogene Himalayan weathering history and river Sr-87/Sr-86: impact on the marine Sr record. Earth and Planetary Science Letters 142 (1–2), 59–74.

Dickinson, W.R., 1970. Interpreting detrital modes of graywacke and arkose. Journal of Sedimentary Petrology 40, 695–707.

Dickinson, W.R., 2008. Impact of differential zircon fertility of granitoid basement rocks in North America on age populations of detrital zircons and implications for granite petrogenesis. Earth and Planetary Science Letters 275 (1–2), 80–92.

Dickinson, W.R., Gehrels, G.E., 2003. U–Pb ages of detrital zircons from Permian and Jurassic eolian sandstones of the Colorado Plateau, USA: paleogeographic implications. Sedimentary Geology 163 (1–2), 29–66.

Dickinson, W.R., Gehrels, G.E., 2008. Sediment delivery to the Cordilleran foreland basin: insights from U–Pb ages of detrital zircons in Upper Jurassic and Cretaceous strata of the Colorado Plateau. American Journal of Science 308 (10), 1041–1082.

Dickinson, W.R., Suczek, C.A., 1979. Plate tectonics and sandstone compositions. AAPG Bulletin 63 (12), 2164–2182.

Dickinson, W.R., Beard, L.S., Brackenbridge, G.R., Erjavec, J.L., Ferguson, R.C., Inman, K.F., Knepp, R.A., Lindberg, F.A., Ryberg, P.T., 1983. Provenance of North-American Phanerozoic sandstones in relation to tectonic setting. Geological Society of America Bulletin 94 (2), 222–235.

Dickinson, W.R., Lawton, T.F., Gehrels, G.E., 2009. Recycling detrital zircons: a case study from the Cretaceous Bisbee Group of southern Arizona. Geology 37 (6), 503–506.

England, P., Molnar, P., 1990. Surface uplift, uplift of rocks, and exhumation of rocks. Geology 18, 1173–1177.

Eriksson, K.A., Campbell, I.H., Palin, J.M., Allen, C.M., 2003. Predominance of Grenvillian magmatism recorded in detrital zircons from modern Appalachian rivers. Journal of Geology 111 (6), 707–717.

Fedo, C.M., Nesbitt, H.W., Young, G.M., 1995. Unraveling the effects of potassium metasomatism in sedimentary rocks and paleosols, with implications for paleoweathering conditions and provenance. Geology 23 (10), 921–924.

Fedo, C.M., Sircombe, K.N., Rainbird, R.H., 2003. Detrital zircon analysis of the sedimentary record. In: Hanchar, J.M., Hoskin, P.W.O. (Eds.), Zircon: Reviews in Mineralogy & Geochemistry, pp. 277–303.

Folk, R.L., 1980. Petrology of sedimentary rocks. Hemphill Publishing Company, Austin, Texas, 184 pp.Galehouse, J.S., 1971. Point counting. In: Carver, R.E. (Ed.), Procedures in Sedimentary Petrology. Wiley Interscience, New York, pp. 385–407.

Gallagher, K., Brown, R., Johnson, C., 1998. Fission track analysis and its applications to geological problems. Annual Review of Earth and Planetary Sciences 26, 519–572.

Garzanti, E., Ando, S., Vezzoli, G., 2008. Settling equivalence of detrital minerals and grain-size dependence of sediment composition. Earth and Planetary Science Letters 273 (1–2), 138–151.

Garzanti, E., Ando, S., Vezzoli, G., 2009. Grain-size dependence of sediment composition and environmental bias in provenance studies. Earth and Planetary Science Letters 277 (3–4), 422–432.

Garzanti, E., Resentini, A., Vezzoli, G., Andò, S., Malusà, M.G., Padoan, M., Paparella, P., 2010. Detrital fingerprints of fossil continental-subduction zones (Axial Belt Provenance, European Alps). Journal of Geology 118 (4), 341–362.

Garzione, C.N., Ikari, M.J., Basu, A.R., 2005. Source of Oligocene to Pliocene sedimentary rocks in the Linxia basin in northeastern Tibet from Nd isotopes: implications for tectonic forcing of climate. Geological Society of America Bulletin 117 (9–10), 1156–1166.

Gazzi, P., 1966. I minerali pesanti nei flysch arenacei fra Monte Ramaceto e Monte Molinatico (Appennino settentrionale). Mineralogica et Petrographica Acta 11, 197–212.

Gehrels, G.E., Yin, A., Wang, X.F., 2003. Detrital-zircon geochronology of the northeastern Tibetan plateau. Geological Society of America Bulletin 115 (7), 881–896.

Gehrels, G., Valencia, V., Pullen, A., 2006. Detrital zircon geochronology by laser-ablation multicollector ICPMS at the Arizona Laserchron Center. In: Olszewski, T. (Ed.), Geochronology: Emerging Opportunities. Paleontological Society, Philadelphia.

Goldstein, S., Arndt, N.T., Stallard, R.F., 1997. The history of a continent from U–Pb ages of zircons from Orinoco River sand and Sm–Nd isotopes in Orinoco basin river sediments. Chemical Geology 139, 271–286.

Gómez, E., Jordan, T.E., Allmendinger, R.W., Hegarty, K., Kelley, S., Heizler, M., 2003. Controls on architecture of the Late Cretaceous to Cenozoic southern Middle Magdalena Valley Basin, Colombia. Geological Society of America Bulletin 115 (2), 131–147.

Gómez, E., Jordan, T.E., Allmendinger, R.W., Hegarty, K., Kelley, S., 2005. Syntectonic Cenozoic sedimentation in the northern middle Magdalena Valley Basin of Colombia and implications for exhumation of the Northern Andes. Geological Society of America Bulletin 117 (5–6), 547–569.

Gregory-Wodzicki, K.M., 2000. Uplift history of the Central and Northern Andes: a review. Geological Society of America Bulletin 112 (7), 1091–1105.

Horton, B.K., Schmitt, J.G., 1998. Development and exhumation of a Neogene sedimentary basin during extension, east-central Nevada. Geological Society of America Bulletin 110 (2), 163–172.

Horton, B.K., Parra, M., Saylor, J.E., Nie, J., Mora, A., Torres, V., Stockli, D.F., Strecker, M.R., 2010a. Resolving uplift of the northern Andes using detrital zircon age signatures. GSA Today 20 (7), 4–9.

Horton, B.K., Saylor, J.E., Nie, J., Mora, A., Parra, M., Reyes-Harker, A., Stockli, D.F., 2010b. Linking sedimentation in the northern Andes to basement configuration, Mesozoic extension, and Cenozoic shortening: evidence from detrital zircon U–Pb ages, Eastern Cordillera, Colombia. Geological Society of America Bulletin 122 (9–10), 1423–1442.

Hoskin, P.W.O., Ireland, T.R., 2000. Rare earth element chemistry of zircon and its use as a provenance indicator. Geology 28 (7), 627–630.

Ingersoll, R.V., Bulard, T.F., Ford, R.L., Grimn, J.P., Pickle, J.P., Sares, S.W., 1984. The effect of grain-size on detrital modes—a test of the Gazzi–Dickinson point-counting method. Journal of Sedimentary Petrology 54 (1), 103–116.

Johnson, C.M., Winter, B.L., 1999. Provenance analysis of lower Paleozoic cratonic quartz arenites of the North American midcontinent region: U–Pb and Sm–Nd isotope geochemistry. Geological Society of America Bulletin 111 (11), 1723–1738.

Johnsson, M.J., 1993. The system controlling the composition of elastic sediments. In: Johnsson, M., B. A. (Eds.), Processes Controlling the Composition of Clastic Sediments. Geological Society of America, Boulder, Colorado, pp. 1–19.

Johnsson, M.J., Stallard, R.F., Meade, R.H., 1988. First-cycle quartz arenites in the Orinoco River basin, Venezuela and Colombia. Journal of Geology 96, 263–277.

Johnston, S., Gehrels, G., Valencia, V., Ruiz, J., 2009. Small-volume U–Pb zircon geochronology by laser ablation–multicollector-ICP-MS. Chemical Geology 259 (3–4), 218–229.

Kempf, O., Blisniuk, P.M., Wang, S., Fang, X., Wrozyna, C., Schwalb, A., 2009. Sedimentology, sedimentary petrology, and paleoecology of the monsoon-driven, fluvio-lacustrine Zhada Basin, SW-Tibet. Sedimentary Geology 222 (1–2), 27–41.

Komar, P.D., 2007. The entrainment, transport, and sorting of heavy minerals by waves and currents. In: Mange, M.A., Wright, D.T. (Eds.), Heavy minerals in use. Elsevier, Amsterdam, pp. 3–48.

Koschinsky, A., Fritsche, U., Winkler, A., 2001. Sequential leaching of Peru Basin surface sediment for the assessment of aged and fresh heavy metal associations and mobility. Deep Sea Research Part II: Topical Studies in Oceanography 48 (17–18), 3683–3699.

Lawrence, R.L., Cox, R., Mapes, R.W., Coleman, D.S., 2011. Hydrodynamic fractionation of zircon age populations. Geological Society of America Bulletin 123, 295–305.

Lawton, T.F., Hunt, G.J., Gehrels, G.E., 2010. Detrital zircon record of thrust belt unroofing in Lower Cretaceous synorogenic conglomerates, central Utah. Geology 38 (5), 463–466.

Link, P.K., Fanning, C.M., Beranek, L.P., 2005. Reliability and longitudinal change of detrital-zircon age spectra in the Snake River system, Idaho and Wyoming: an example of reproducing the bumpy barcode. Sedimentary Geology 182 (1–4), 101–142.

Linn, A.M., Depaolo, D.J., Ingersoll, R.V., 1992. Nd–Sr isotopic, geochemical, and petrographic stratigraphy and paleotectonic analysis: Mesozoic Great Valley forearc sedimentary rocks of California. Geological Society of America Bulletin 104 (10), 1264–1279.

Ludwig, K.R., 2003. User's Manual for Isoplot 3.00 a Geochronological Toolkit for Microsoft Excel.

Mange, M.A., Maurer, H.F.W., 1992. Heavy Minerals in Colour. Chapman and Hall, London.

Mange, M.A., Otvos, E.G., 2005. Gulf coastal plain evolution in West Louisiana: heavy mineral provenance and Pleistocene alluvial chronology. Sedimentary Geology 182 (1–4), 29–57.

Mange, M.A., Wright, D.T.I.E., 2007. High-resolution heavy mineral analysis (HRHMA): a brief summary. In: Mange, M.A., Wright, D.T. (Eds.), Developments in Sedimentology, 58. Elsevier, Amsterdam, pp. 433–436.

Mange, M.A., Dewey, J.F., Floyd, J.D., 2005. The origin, evolution and provenance of the Northern Belt (Ordovician) of the Southern Uplands Terrane, Scotland: a heavy mineral perspective, pp. 251–280.

Mange-Rajetzky, M.A., 1995. Subdivision and correlation of monotonous sandstone sequences using high-resolution heavy mineral analysis, a case study: the Triassic of the Central Graben. Geological Society, London, Special Publications 89 (1), 23–30.

McClelland, W.C., Gehrels, G.E., Samson, S.D., Patchett, P.J., 1992. Structural and geochronological relations along the western flank of the coast mountains batholith—Stikine river to Cape Fanshaw, central southeastern Alaska. Journal of Structural Geology 14 (4), 475–489.

McCourt, W.J., Aspden, J.A., Brook, M., 1984. New geological and geochronological data from the Colombian Andes—Continental growth by multiple accretion. Geological Society of London Journal 141, 831–845. doi:10.1144/gsjgs.141.5.0831.

McLennan, S.M., 1989. Rare earth elements in sedimentary rocks; influence of provenance and sedimentary processes. Reviews in Mineralogy 21, 169–200.

Milliken, K.L., 1988. Loss of provenance information through subsurface diagenesis in Plio-Pleistocene sandstones, northern Gulf of Mexico. Journal of Sedimentary Petrology 58 (6), 992–1002.

Moecher, D.P., Samson, S.D., 2006. Differential zircon fertility of source terranes and natural bias in the detrital zircon record: Implications for sedimentary provenance analysis. Earth and Planetary Science Letters 247 (3–4), 252–266.

Mora, A., Parra, M., Strecker, M., Kammer, A., Dimaté, C., Rodríguez, F., 2006. Cenozoic contractional reactivation of Mesozoic extensional structures in the Eastern Cordillera of Colombia. Tectonics 25 (2), TC2010. doi:10.1029/2005TC001854.

Mora, A., Parra, M., Strecker, M.R., Sobel, E.R., Hooghiemstra, H., Torres, V., Jaramillo, J.V., 2008. Climatic forcing of asymmetric orogenic evolution in the Eastern Cordillera of Colombia. Geological Society of America Bulletin 120 (7–8), 930–949.

Morales, L., 1958. General geology and oil occurrences of Middle Magdalena Valley, Colombia. In: Weeks, L.G. (Ed.), Habitat of Oil Symposium: AAPG Special Publication, pp. 641–695.

Moreno, C.J., Horton, B.K., Caballero, V., Mora, A., Parra, M., Sierra, J., 2011. Depositional and provenance record of the Paleogene transition from foreland to hinterland basin evolution during Andean orogenesis, northern Middle Magdalena Valley Basin, Colombia. Journal of South American Earth Sciences 32.

Morton, A.C., 1985. Heavy minerals in provenance studies. In: Zuffa, G.G. (Ed.), Provenance of Arenites. Reidel, Dordrecht, pp. 249–277.

Morton, A.C., Hallsworth, C., 1994. Identifying provenance-specific features of detrital heavy mineral assemblages in sandstones. Sedimentary Geology 90 (3–4), 241–256.

Morton, A.C., Hallsworth, C.R., 1999. Processes controlling the composition of heavy mineral assemblages in sandstones. Sedimentary Geology 124 (1–4), 3–29.

Najman, Y., Garzanti, E., 2000. Reconstructing early Himalayan tectonic evolution and paleogeography from Tertiary foreland basin sedimentary rocks, northern India. Geological Society of America Bulletin 112 (3), 435–449.

Najman, Y., Bickle, M., Garzanti, E., Pringle, M., Barfod, D., Brozovic, N., Burbank, D., Ando, S., 2009. Reconstructing the exhumation history of the Lesser Himalaya, NW India, from a multitechnique provenance study of the foreland basin Siwalik Group. Tectonics 28, TC5018. doi:10.1029/2009TC002506.

Nesbitt, H.W., Young, G.M., 1996. Petrogenesis of sediments in the absence of chemical weathering: effects of abrasion and sorting on bulk composition and mineralogy. Sedimentology 43 (2), 341–358.

Nie, J., Horton, B.K., Mora, A., Saylor, J.E., Housh, T.B., Rubiano, J., Naranjo, J., 2010. Tracking exhumation of Andean ranges bounding the Middle Magdalena Valley Basin, Colombia. Geology 451–454.

Niemi, N.A., Wernicke, B.P., Brady, R.J., Saleeby, J.B., Dunne, G.C., 2001. Distribution and provenance of the middle Miocene Eagle Mountain Formation, and implications for regional kinematic analysis of the Basin and Range province. Geological Society of America Bulletin 113 (4), 419–442.

Ohta, T., 2008. Measuring and adjusting the weathering and hydraulic sorting effects for rigorous provenance analysis of sedimentary rocks: a case study from the Jurassic Ashikita Group, south-west Japan. Sedimentology 55 (6), 1687–1701.

Parra, M., Mora, A., Sobel, E.R., Strecker, M.R., Gonzalez, R., 2009. Episodic orogenic front migration in the northern Andes: constraints from low-temperature thermochronology in the Eastern Cordillera, Colombia. Tectonics 28.

Pe-Piper, G., Triantafyllidis, S., Piper, D.J.W., 2008. Geochemical identification of clastic sediment provenance from known sources of similar geology: the cretaceous Scotian Basin, Canada. Journal of Sedimentary Research 78 (9–10), 595–607.

Pindell, J.L., Kennan, L., Wright, D., Erikson, J., 2009. Clastic domains of sandstones in central/eastern Venezuela, Trinidad, and Barbados: heavy mineral and tectonic constraints on provenance and palaeogeography. In: James, K.H., Lorente, M.A., Pindell, J.L. (Eds.), Origin and Evolution of the Caribbean Plate: Geological Society Special Publication, pp. 743–797.

Priem, H.N.A., Kroonenberg, S.B., Boelrijk, N., Hebeda, E.H., 1989. Rb–Sr and K–Ar evidence for the presence of a 1.6 Ga basement underlying the 1.2 Ga Garzón–Santa Marta granulite belt in the Colombian Andes. Precambrian Research 42 (3–4), 315–324.

Rainbird, R.H., Heaman, L.M., Young, G., 1992. Sampling Laurentia: detrital zircon geochronology offers evidence for an extensive Neoproterozoic river system originating from the Grenville orogen. Geology 20 (4), 351–354.

Rangel, A., Moldowan, J.M., Nino, C., Parra, P., Giraldo, B.N., 2002. Umir Formation: organic geochemical and stratigraphic assessment as cosource for Middle Magdalena Basin oil, Colombia. AAPG Bulletin 86 (12), 2069–2087.

Reiners, P.W., Campbell, I.H., Nicolescu, S., Allen, C.M., Hourigan, J.K., Garver, J.I., Mattinson, J.M., Cowan, D.S., 2005. (U–Th)/(He–Pb) double dating of detrital zircons. American Journal of Science 305 (4), 259–311.

Restrepo-Pace, P.A., Ruiz, J., Gehrels, G., Cosca, M., 1997. Geochronology and Nd isotopic data of Grenville-age rocks in the Colombian Andes: new constraints for Late Proterozoic–Early Paleozoic paleocontinental reconstructions of the Americas. Earth and Planetary Science Letters 150 (3–4), 427–441.

Riggs, N.R., Lehman, T.M., Gehrels, G.E., Dickinson, W.R., 1996. Detrital zircon link between headwaters and terminus of the upper Triassic Chinle–Dockum paleoriver system. Science 273 (5271), 97–100.

Robinson, D.M., DeCelles, P.G., Patchett, P.J., Garzione, C.N., 2001. The kinematic evolution of the Nepalese Himalaya interpreted from Nd isotopes. Earth and Planetary Science Letters 192 (4), 507–521.

Roser, B.P., Korsch, R.J., 1988. Provenance signatures of sandstone mudstone suites determined using discriminant function-analysis of major-element data. Chemical Geology 67 (1–2), 119–139.

Ross, G.M., Parrish, R.R., Winston, D., 1992. Provenance and U–Pb geochronology of the Mesoproterozoic belt supergroup (Northwestern United-States)—implications for age of deposition and pre-Panthalassa plate reconstructions. Earth and Planetary Science Letters 113 (1–2), 57–76.

Sarmiento-Rojas, L.F., Van Wess, J.D., Cloetingh, S., 2006. Mesozoic transtensional basin history of the Eastern Cordillera, Colombian Andes: inferences from tectonic models. Journal of South American Earth Sciences 21 (4), 383–411.

Saylor, J.E., Mora, A., Horton, B.K., Nie, J., 2009. Controls on the isotopic composition of surface water and precipitation in the northern Andes, Colombian Eastern Cordillera. Geochimica et Cosmochimica Acta 73, 6999–7018.

Saylor, J.E., Horton, B.K., Nie, J., Corredor, J., Mora, A., 2011. Evaluating foreland basin partitioning in the northern Andes using Cenozoic fill of the Floresta basin, Eastern Cordillera, Colombia. Basin Research 23, 377–402.

Steidtmann, J.R., Schmitt, J.G., 1988. Provenance and dispersal of tectogenic sediments in thin-skinned, thrusted terrains. In: Kleinspehn, K.L., Paola, C. (Eds.), New Perspectives in Basin Analysis. Springer-Verlag, New York, pp. 353–366.

Suttner, L.J., Basu, A., 1985. The effect of grain-size on detrital modes—a test of the Gazzi–Dickinson point-counting method—discussion. Journal of Sedimentary Petrology 55 (4), 616–617.

Suttner, L.J., Basu, A., Mack, G.H., 1981. Climate and the origin of quartz arenites. Journal of Sedimentary Petrology 51 (4), 1235–1246.

Taylor, S.R., McLennan, S.M., 1985. The Continental Crust: Its Composition and Evolution. Blackwell, Cambridge. 312 pp.

Teixeira, W., Tassinari, C.C.G., Cordani, U.G., Kawashita, K., 1989. A review of the geochronology of the Amazonian craton—tectonic implications. Precambrian Research 42 (3–4), 213–227.

Thomas, W.A., Astini, R.A., Mueller, P.A., Gehrels, G.E., Wooden, J.L., 2004. Transfer of the Argentine Precordillera terrane from Laurentia: constraints from detrital-zircon geochronology. Geology 32 (11), 965–968.

Uddin, A., Lundberg, N., 1998. Unroofing history of the eastern Himalaya and the Indo-Burman ranges: heavy-mineral study of Cenozoic sediments from the Bengal Basin, Bangladesh. Journal of Sedimentary Research 68 (3), 465–472.

Vermeesch, P., 2004. How many grains are needed for a provenance study? Earth and Planetary Science Letters 224, 441–451.

Vezzoli, G., Forno, M.G., Andò, S., Hron, K., Cadoppi, P., Rossello, E., Tranchero, V., 2010. Tracing the drainage change in the Po basin from provenance of Quaternary sediments (Collina di Torino, Italy). Quaternary International 222 (1–2), 64–71.

Villagómez, D., 2010. Thermochronology, geochronology and geochemistry of the Western and Central cordilleras and Sierra Nevada de Santa Marta, Colombia: The tectonic evolution of NW South America. University of Geneva, Geneva. 126 pp.

Villamil, T., 1999. Campanian–Miocene tectonostratigraphy, depocenter evolution and basin development of Colombia and western Venezuela. Palaeogeography, Palaeoclimatology, Palaeoecology 153 (1–4), 239–275.

von Eynatten, H., 2003. Petrography and chemistry of sandstones from the Swiss Molasse Basin: an archive of the Oligocene to Miocene evolution of the Central Alps. Sedimentology 50 (4), 703–724.

Weislogel, A.L., Graham, S.A., Chang, E.Z., Wooden, J.L., Gehrels, G.E., Yang, H., 2006. Detrital zircon provenance of the Late Triassic Songpan–Ganzi complex: sedimentary record of collision of the North and South China blocks. Geology 34 (2), 97–100.

Yue, Y.J., Graham, S.A., Ritts, B.D., Wooden, J.L., 2005. Detrital zircon provenance evidence for large-scale extrusion along the Altyn Tagh fault. Tectonophysics 406 (3–4), 165–178.

Zachos, J., Pagani, M., Sloan, L., Thomas, E., Billups, K., 2001. Trends, rhythms, and aberrations in global climate 65 Ma to present. Science 292, 686–693.

Zahid, K.M., Barbeau, D.L., 2010. Provenance of eastern Magallanes foreland basin sediments: heavy mineral analysis reveals Paleogene tectonic unroofing of the Fuegian Andes hinterland. Sedimentary Geology 229 (1–2), 64–74.